

Fragment-Derived Selective Inhibitors of Dual-Specificity Kinases
DYRK1A and DYRK1B

David Lee Walmsley, James B. Murray, Pawel Dokurno, Andrew J. Massey, Karen Benwell, Andrea Fiumana, Nicolas Foloppe, Stuart Ray, Julia Smith, Allan E. Surgenor, Thomas Edmonds, Didier Demarles, Mike Burbridge, Francisco Cruzalegui, Andras Kotschy, and Roderick E. Hubbard*



Cite This: *J. Med. Chem.* 2021, 64, 8971–8991



Read Online

ACCESS |



Metrics & More

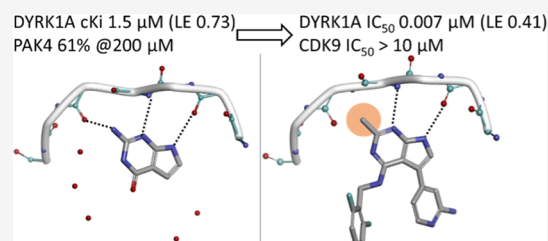


Article Recommendations



Supporting Information

ABSTRACT: The serine/threonine kinase DYRK1A has been implicated in regulation of a variety of cellular processes associated with cancer progression, including cell cycle control, DNA damage repair, protection from apoptosis, cell differentiation, and metastasis. In addition, elevated-level DYRK1A activity has been associated with increased severity of symptoms in Down's syndrome. A selective inhibitor of DYRK1A could therefore be of therapeutic benefit. We have used fragment and structure-based discovery methods to identify a highly selective, well-tolerated, brain-penetrant DYRK1A inhibitor which showed in vivo activity in a tumor model. The inhibitor provides a useful tool compound for further exploration of the effect of DYRK1A inhibition in models of disease.



INTRODUCTION

DYRK1A is the best-studied member of the evolutionarily conserved DYRK (dual-specificity tyrosine-regulated kinase) branch of the cyclin-dependent, mitogen-activated, glycogen synthase, and CDC-like (CMGC) family of serine/threonine kinases that consists of two classes: DYRK1A and DYRK1B (Class 1) and DYRK2, DYRK3, and DYRK4 (Class 2). DYRK1A is activated by self-phosphorylation of S520, leading to 14-3-3 β binding which stimulates the catalytic activity.¹

DYRK1A and 1B play an important role in cell cycle control and modulation of DYRK1A/B in sarcoma,^{2,3} and lung,⁴ pancreatic,⁵ and ovarian cancer⁶ can result in dysregulation of cell cycle control. These kinases regulate the induction of quiescence via control of the DREAM complex,⁷ thereby controlling the G0-G1 transition and exit from quiescence.^{8–10}

DYRK1A and 1B can also phosphorylate Cyclin D1 (resulting in its destabilization)^{11,12} and p27Kip1,^{13,14} thereby altering the cell's decision to enter the cell cycle. Additionally, DYRK1A kinase activity stabilizes epidermal growth factor (EGFR) in glioblastoma through regulation of Sprouty2, and inhibition of DYRK1A reduces EGFR-dependent glioblastoma growth.¹⁵ DYRK1A and 1B control the activity of the Hedgehog signaling effector GLI through direct phosphorylation, resulting in increased nuclear accumulation and transcriptional activity.¹⁶ Pharmacological inhibition of DYRK1B repressed Hedgehog signaling and inhibited the proliferation of GLI1-dependent pancreatic cancer cells.¹⁷ Recent work suggests that suppression of DYRK1A restrains myeloid cell leukemia 1 (MCL-1) expression and sensitizes non-small cell lung cancer cells to B-cell lymphoma 2 (Bcl-2) inhibitors.¹⁸ Of the Class 2 DYRKs, DYRK2 has been

implicated to have multiple roles in cancer development including a role in the G1/S and G2/M cell cycle transition, epithelial–mesenchymal transition, cancer stemness, and DNA damage response through p53 phosphorylation. In lower eukaryotes, DYRK2 has been implicated in tissue development, thereby implying a role for this kinase in cell differentiation and homeostasis in mammals.^{19,20} These observations suggest that targeting DYRK kinase activity could be of therapeutic benefit for patients presenting with a diverse range of cancers.

There has also been interest in DYRK1A in patients with Down's syndrome. The gene is located on chromosome 21, and the subsequent elevated levels of DYRK1A in Down's syndrome patients has been correlated with an increase in severity of symptoms and a poorer prognosis.²¹ Recently, it has been suggested that a natural product inhibitor of DYRK1A, the polyphenol from green tea, epigallocatechin gallate (EGCG), has efficacy in a murine model of Down's syndrome through chromosome 16 trisomy.²² Although the wider activity, instability, and poor compound properties of EGCG complicate interpretation of these results, inhibiting DYRK kinase activity could also be of therapeutic benefit to Down's syndrome patients.

In addition to Down's syndrome, recent studies have suggested a role for DYRK1A in other neurodegenerative

Received: January 7, 2021

Published: June 18, 2021



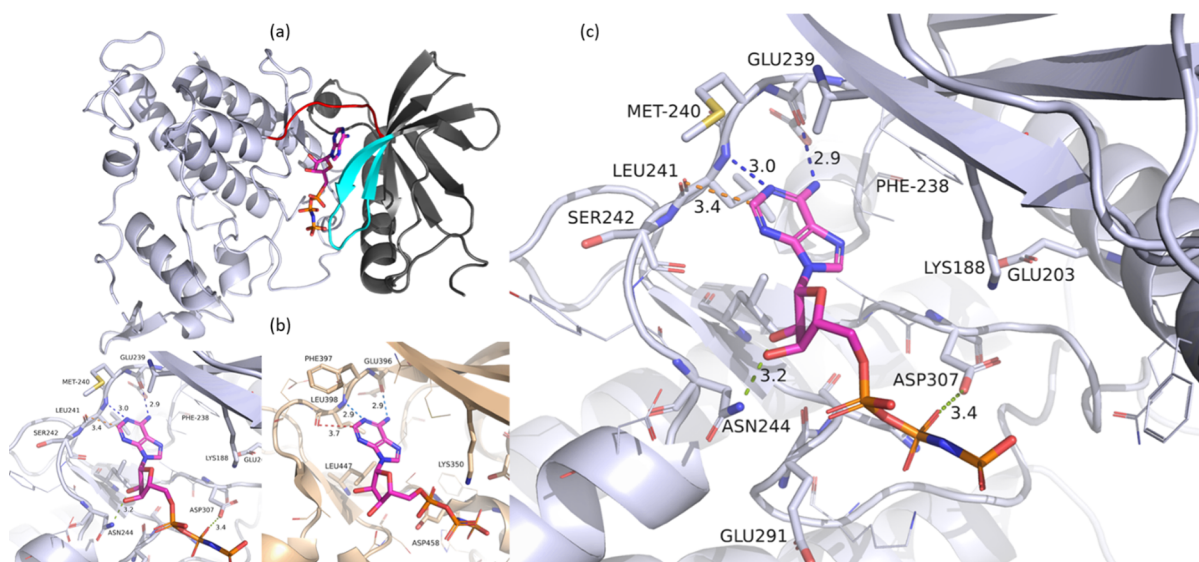


Figure 1. (a) Ribbon structure of Dyrk1a, highlighting hinge (red) and ADPNP bound in the stick (monomer B in the crystal structure, PDB: 7A4O) and the portion of the structure (light blue) removed in all subsequent figures (residues E160 to D178 which include the glycine loop). (b) Closeup of the ATP binding site showing side by side ADPNP bound to Dyrk1a (main chain white) and PAK4 (main chain pink) (PDB: 4FIG). (c) Standard orientation and convention (unless stated) used for figures of compounds (element coloring with purple carbons) binding to Dyrk1a—remove the glycine loop from E160 to D178 to view compound binding, peptide backbone as a ribbon structure for the remainder of the protein except for Dyrk1a F238 to N244 (hinge region) and V306 to F308 with additional selected side chains and water molecules (none in Figure 1) colored on the element in stick (gray carbons) and protein backbone and side chain hydrogen bonds as blue and green dashed lines with nonstandard interactions in orange dashed lines.

disorders such as Alzheimer's disease (including early onset AD in Down's syndrome patients^{23–25}) and Parkinson's disease.^{26,27} DYRK1A has also been demonstrated to regulate the proliferation and cell size of beta cells (and therefore their regenerative capacity) in the pancreas^{28–30}.

Our objective was to use fragment and structure-based lead discovery methods to identify potent and selective adenosine triphosphate (ATP) competitive inhibitors of DYRK1A and DYRK1B to be used to probe the therapeutic benefit of inhibiting this class of kinase. Our work was initiated concurrently to the release of the first structure of the kinase domain of DYRK1A (protein databank (PDB) code 2VX3³¹) by the Structural Genomics Consortium in 2009. Here, we describe the initial fragment-based hit discovery efforts that identified multiple series of hit compounds and the lead optimization aided by molecular modeling that generated pyrrolopyrimidine compounds that were profiled in several cellular and *in vivo* models. An accompanying paper³² describes a companion optimization project to generate imidazopyridine compounds that were similarly profiled. DYRK1A and DYRK1B vary by only one amino acid in the ATP-binding pocket; the Class 2 DYRKs have more variation.

The lead molecule, **34**, from this pyrrolopyrimidine hit series inhibited DYRK1A and 1B with low nM potency and exhibited excellent selectivity versus the Class 2 DYRKs. It potently inhibited DYRK1A autophosphorylation in a cellular model and had good oral bioavailability with a robust pharmacokinetic (PK)/pharmacodynamic (PD) relationship with *in vivo* activity in a glioblastoma xenograft model. This molecule is a potentially useful tool compound for further study of the effect of DYRK1A inhibition in models of human disease.

RESULTS AND DISCUSSION

Fragment screening and structural studies used a construct of the DYRK1A kinase domain (hereafter termed Dyrk1a) similar

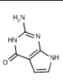
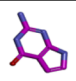
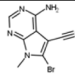
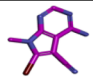
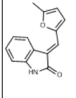
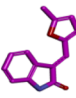
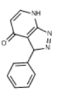
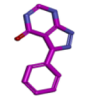
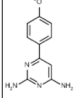

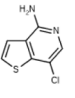
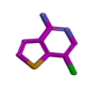
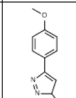
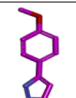
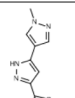
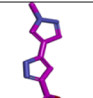
to that used to generate the crystal structure deposited with PDB code 2vx3³¹ (see the Experimental Section for details). The kinase p21-associated kinase 4 (4PAK4) was used as a counterscreen throughout the project, and selectivity against other kinases was measured as the project progressed. The inhibition of a selection of protein kinases was measured using either an adenosine diphosphate (ADP) Hunter or time-resolved fluorescence energy transfer (TR-FRET) assay, and the inhibition of GSK3- β was measured by a radiometric assay (details in the Experimental Section).

We solved the crystal structure of Dyrk1a with 5'-adenylyl- β , γ -imidodiphosphate (ADPNP) bound. Figure 1 shows a comparison between this structure of Dyrk1a and the published structure of PAK4 with ADPNP.³³

Dyrk1a has the conventional fold of a protein kinase with a larger, predominantly α -helical subdomain connected to a predominantly β -sheet subdomain, forming a cleft that binds ATP. The subdomains are connected by a so-called "hinge" region where the main chain atoms hydrogen-bond to the donor–acceptor–donor motif of the adenosine moiety of ATP, positioning the sugar and phosphate groups adjacent to the catalytic machinery. The structure reveals an unusual conformation for the main chain carbonyl of L241 in Dyrk1a compared to that seen for the equivalent amino acid (L398) in PAK4 (Figure 1b) and other kinases (data not shown).

Identifying and Characterizing the Initial Fragment Hits. The Vernalis fragment library consisting of 1063 compounds at the time^{34,35} was screened using three ligand-observed nuclear magnetic resonance (NMR) experiments³⁶ for binding to the ATP-binding site of Dyrk1a in competition with the nonspecific kinase inhibitor, staurosporine. Compounds that were confirmed as binding competitively in all three NMR experiments were assayed in an ADP Hunter biochemical assay (hereafter the functional assay) to generate 166 fragment hits, a hit rate of 15%.

Table 1. Fragment Hits Ranked by Ligand Efficiency Measured in ADP Hunter Assay

Number	structure	DYRK1a cKi μM (LE)	PAK4 inhibition ^a	crystal structure ^a	Number	structure	DYRK1a cKi μM (LE)	PAK4 inhibition ^a	crystal structure ^a
1		1.5 (0.73)	61%		5		6.4 (0.51)	55%	
2		4.4 (0.67)	28% ^a		6		2.3 (0.48)	46	
3		0.1 (0.59)	7%		7		1.5 (0.47)	23%	
4		6.1 (0.51)	48% ^a		8		>200	6%	

^a% inhibition in PAK4 assay with the 200 μM (400 μM) compound; binding pose in the crystal structure in the same orientation as Figure 1c. See Tables S1 and S2 for structure determination and refinement statistics; the accession codes for coordinates deposited to the PDB are listed at the end of the manuscript. All 2D chemical structures are oriented to approximate the binding pose seen in crystal structures.

Table 1 lists the 8 hits with the highest ligand efficiency [LE,³⁷ defined as free energy of binding (ΔG)/heavy atom count (HAC)]. A high hit rate in an NMR fragment screen indicates^{38,39} a highly efficient site for binding small molecules (often termed druggable⁴⁰), and the high LE of the hits reinforces this for the ATP binding site in Dyrk1a. In addition, these fragment hits show remarkable selectivity, given some contain relatively standard kinase ATP binding motifs. This can be explained by inspection of the Dyrk1a structure (Figure 1c) which shows a distinctive conformation for the carbonyl of the hinge amino acid, L241.

We determined the crystal structures for the eight fragment hits bound to Dyrk1a (Tables 1, S1 and S2). The fragments exhibited both “classical” hinge binding with a donor–acceptor–donor hydrogen bonding motif and “nonclassical” where as few as one hydrogen bond anchors the fragment to the hinge in the binding site. This diversity of binding modes and motifs demonstrates one of the benefits of fragment-based discovery: even for the widely studied ATP binding site of a kinase, a fragment screen can identify compounds that explore features that can be exploited for selectivity, identify novel binding modes that are not often discovered when screening larger compounds, and provide a wide diversity of hit compounds from which the medicinal chemist can choose the most appropriate one for optimization.

As the fragment screen was completed, the crystal structure (PDB: 3ANR) and properties of harmine (9) on Dyrk1a were published⁴¹ and the activity of meriolin derivatives was reported.⁴²

Figure 2 compares the binding of harmine (9) and meriolin-3 (10) to Dyrk1a with some of the fragment hits. As shown in Figure 2a, fragment 3 and harmine both have a “nonclassical” binding mode, making just one hydrogen bond to the hinge and with the methyl group of the methoxy in the pocket formed by the unusual conformation of the main chain of L241 and one to E203. This fragment is very similar to fragment 4. The optimization of fragment 3 with a similar binding mode to harmine is described in a separate publication.³² The fragment 1 (Figure 2b) makes a “classical” set of hydrogen bonds with the hinge, overlapping with the core of 10 which also interacts

with E203 through the NH_2 of the pendant amino pyrimidine (Figure 2b). Fragment 5 (Figure 2c) was selected for further study as it makes a comprehensive set of interactions not only with the hinge but also with the catalytic residues at the base of the binding site through a well-defined network of hydrogen bonds to water.

Optimization from the Fragment to Lead Pyrrolopyrimidine Series. The first step of optimization was to exploit the pocket proximal to the carbonyl of L241. Inspection of the crystal structures (Figure 2) suggested that a methyl group could be incorporated into the 2-position of the pyrrolopyrimidine scaffold of 5. As can be seen in Table 2, this improved the affinity of compounds for DYRK1A and retained selectivity over PAK4. We also investigated substitution of the 6-position bromine with various aryls and heteroaryl to improve potency further by building groups that replaced the solvent to interact with K188 and E203.

The crystal structure (Figure 3) of the most ligand-efficient compound of the series (16) bound to Dyrk1a confirmed the success of the structure-based design and the structural basis for retention of good selectivity against PAK4. The 2-methyl occupies the pocket adjacent to carbonyl of L241, and the pyridine nitrogen hydrogen-bonds to K188 with the other polar atoms of the ligand making interactions with defined solvent positions.

It was noted in the structures of 10 (Figure 2b) and the most ligand efficient fragment (1) that the 4-amino group of the pyrimidine ring of 16 is within a pyrrole ring, making a “classical” hinge binding interaction with the carbonyl of E239. A series of 2-methyl-5-aryl-7H-pyrrolo[2,3-d]pyrimidines were therefore synthesized as listed in Table 3, keeping the methyl group to target the L241 pocket and designed to retain the main interactions with the remainder of the binding site. A 4-position methoxy was also included for further elaboration.

The three most potent compounds (18, 19, and 20) were profiled for their inhibition of a mini-panel of kinases (Table 4).

The most potent compound (19) combines high target affinity (and LE of 0.57), almost equipotent inhibition of the other profiled DYRK enzymes and with good selectivity against

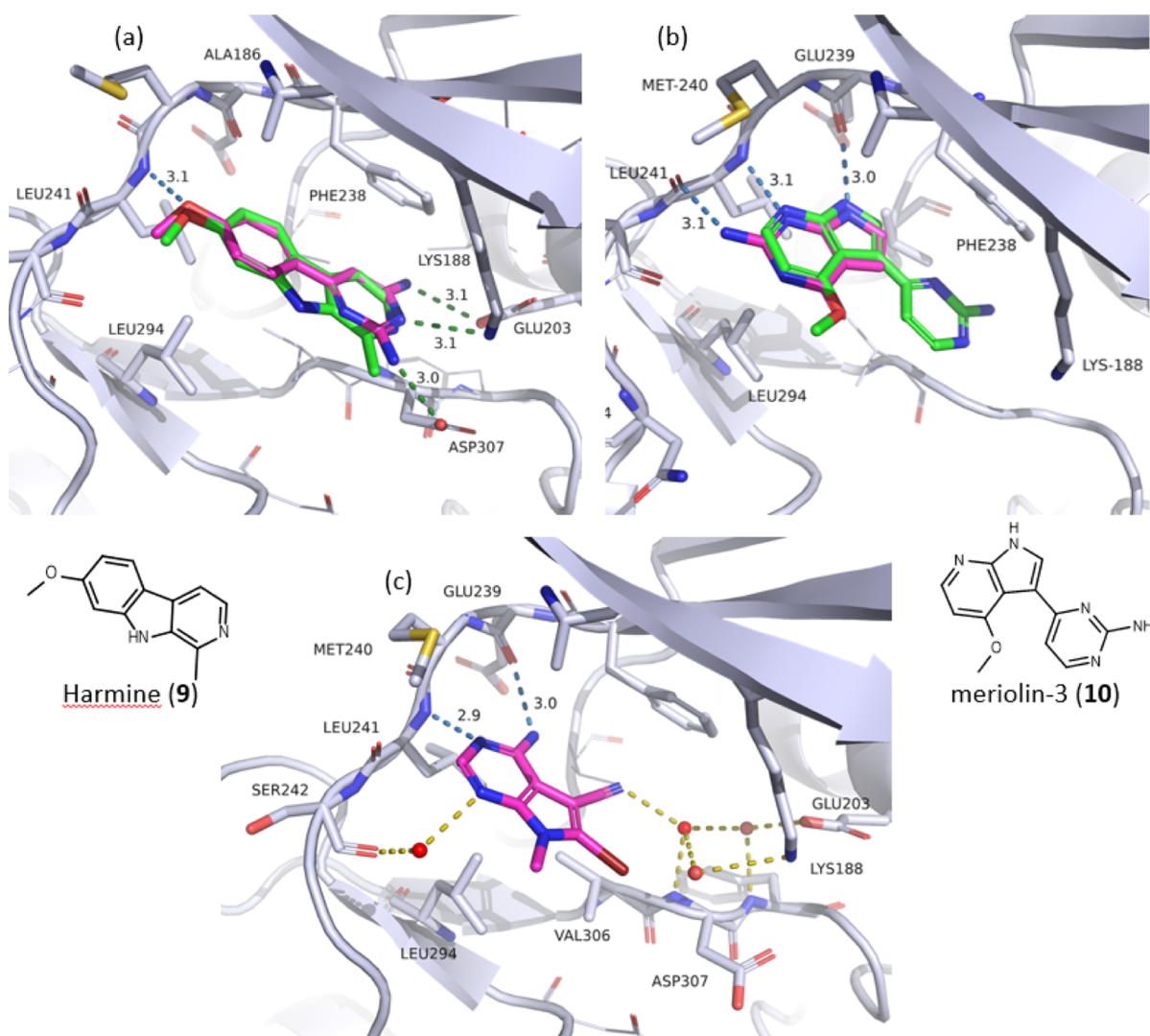


Figure 2. Detailed comparison of the binding mode of literature compounds and selected fragments to Dyrk1a showing the protein structure (white ribbon), selected waters, and key interactions with the fragment (a) harmine (**9**—green carbons, PDB: 3ANR) and fragment 3 (PDB: 7A4W); (b) meriolin-3 (**10**—green carbons, PDB: 7A5B) and fragment 1 (PDB: 7A4R); and (c) fragment 5 (PDB: 7A51). See the legend to Figure 1 for conventions used in the representation.

other kinases. The 4-position methoxy on the pyrimidine presents a vector toward the amino acids in the sugar pocket of the ATP site and the glycine loop regions. A selection of single-ring aromatic moieties were synthesized at this 4-position (Table 5).

Simple aromatics such as thiophene (**24**) achieve single-digit nanomolar potency in the DYRK1A functional assay, more than 2 orders of magnitude greater than inhibition of Gsk3 β and cyclin-dependent kinase 9 (CDK9). The crystal structure of **24** (Figure 4) bound to Dyrk1a confirmed the predicted interactions that were made with additional Van Der Waals interactions made in a lipophilic region under the glycine loop (not shown in Figure 4) contributed to by G168 and the side chains of I165, F170, V173, and K188. However, the 4-alkoxy compounds were unstable in aqueous media at pH < 5 over a relatively short period of a few hours due to hydrolysis of the pendant methoxy (as analyzed by liquid chromatography–mass spectrometry, LCMS), presumably via protonation of the pyrimidine ring.

Similar benzylic motifs were introduced to make glycine loop interactions by installing benzylamines at the 4-position.

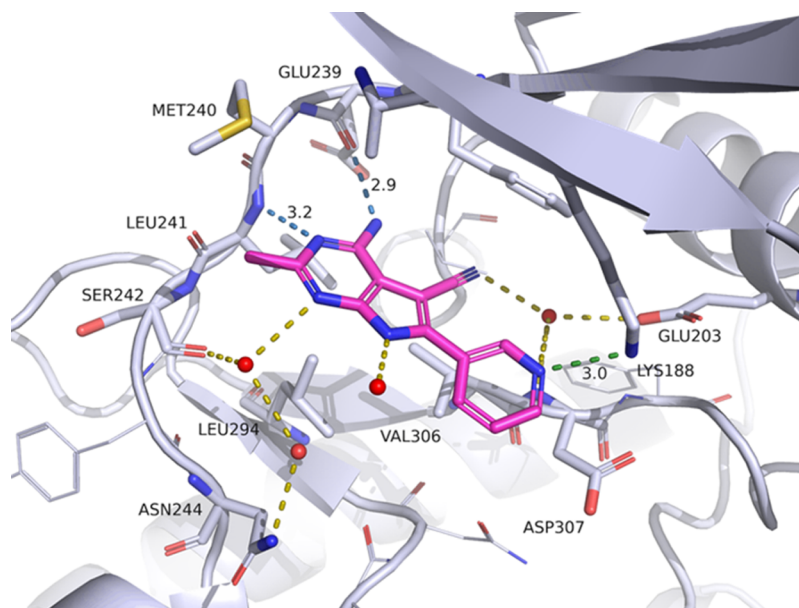
A number of 5-membered heterocycles had similar potency and selectivity (Table 6) and were found to be stable under a range of aqueous conditions.

Lead Optimization to the Compound Suitable for *in Vivo* Studies. The next stage in optimization was to investigate further substituents at the 4-position of the pyrimidine aromatic ring. A number of analogues were synthesized, and a biaryl compound (**37**) was introduced by direct coupling. These were all successful in retaining potency but with an altered selectivity profile, particularly against DYRK2. The cellular activity and metabolic stability of this set of compounds were also profiled (Table 7).

As can be seen in Figure 5, introduction of ortho substituents on the pendant benzyl ring induces a twist of the aromatic to be perpendicular to the plane of the pyrrolopyrimidine core. This twist displaces a water molecule in the structure. **34** was taken as the most promising lead compound. Although the metabolic stability is moderate, it shows good cellular activity with the IC₅₀ for inhibition of the autophosphorylation of S520 on DYRK1A in U2OS cells only threefold less than the IC₅₀ in the functional assay and with an

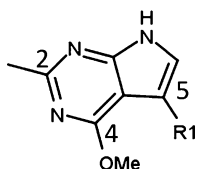
Table 2. Improving Interactions with the Carbonyl of L241 and the Catalytic Site; ND—Not Determined

Compound number	R3	R2	R1	ADP DYRK1A IC ₅₀ μM	ADP DYRK1A cKi	DYRK1A LE	ADP PAK4 IC ₅₀ μM
5	H	Me	Br	12.8	6.4	0.51	>200
11	Me	Et		1.8	0.89	0.40	ND
12	Me	Et		0.25	0.12	0.41	>50
13	Me	Me		0.12	0.059	0.45	>50
14	Me	Me		3.0	1.5	0.36	ND
15	Me	Me		0.38	0.19	0.46	ND
16	Me	H		0.065	0.032	0.54	>50
17	Me	H		0.068	0.034	0.49	>50

Figure 3. Structure of **16** bound to Dyk1a (PDB: 7A5D). See the legend to Figure 1 for conventions used in the representation.

EC₅₀ of less than 1 nM in a nano-BRET assay (Figure S1). These results are consistent with the cell permeability properties of the compound, measured in a Caco2 assay (see Table 7). In addition, the very high plasma protein binding (unbound fraction f_u <1% in mouse and human plasma) should mitigate the measured effect on human ether-a-go-go-related gene (hERG), suggesting that the compound was suitable for further *in vitro* and *in vivo* profiling.

Selectivity. The selectivity profile for inhibition of other protein kinases by **34** was characterized in an Ambit kinase assay which measured the percentage activity remaining for each of 442 kinases (Table S4). Only two kinases were inhibited to less than 10% activity at 10 nM compound, DYRK1A (0.4%) and DYRK1B (5%), and only eight other kinases to less than 90% activity, most notably CLK1 (24%), CLK2 (10%), CLK4 (23%), and HIPK2 (53%), showing

Table 3. Changing to a Pyrrolo[2,3-*d*]pyrimidine Scaffold

Compound Number	R1	ADP DYRK1A IC ₅₀ μ M	ADP DYRK1A cK _i μ M	DYRK1A LE
18		0.05	0.02	0.58
19		0.02	0.01	0.57
20		0.04	0.02	0.55
21		4.8	2.4	0.37
22		0.24	0.12	0.50
23		68% (50 μ M)	25	0.33

excellent selectivity against DYRK2 (88%). At 1 μ M compound, only 15 kinases were inhibited to less than 50% activity. Although IC₅₀ values for compounds inhibiting a particular kinase can be compared, it is more difficult to compare such values across enzymes where there will be different K_M s for ATP, substrate, and assay conditions. We therefore determined the K_d for **34** binding to DYRK1A, DYRK1B, CLK1, CLK2, and CLK4 in a DiscoverX Kinomscan binding assay which gave values of 0.24, 0.05, 2.6, 0.9, and 0.8 nM, respectively, confirming the selectivity for DYRK1A and the high affinity for CLK kinases. An overlay (Figure S2) of a published structure of CLK1 (PDB code 6Q8K⁴³) with that of **34** bound to Dyrk1a shows that L244 in CLK1 (equivalent to L241 in Dyrk1a) adopts a similar conformation, providing some explanation for the observed selectivity, which is a feature seen for other DYRK1A inhibitors.⁴³

Brain Permeability. Preliminary assessment of oral versus iv PK (Figure S3) showed that the compound has moderate oral bioavailability in the mouse (% *F* = 33). Three animals (female SCID mice) were dosed with compound **34** at po 25 mg/kg, and the mean plasma and brain concentrations (2 h after dosing) of the compound were measured as 1849 and 133 ng/mL, respectively (see Table S5). The calculated brain to plasma partition was 0.1.

ADME-PK. Female nude BALB/c mice were dosed po at 25 and 100 mg/kg, and the plasma concentration of **34** was measured as shown in Table 8 (details in Table S6). The

compound was absorbed slowly, giving a C_{max} a few hours after dosing and showing moderate exposure.

In vivo Efficacy. These properties of **34**, namely, kinase selectivity (particularly against DYRK2), moderate exposure, and brain penetration, and the fact that the compound is tolerated *in vivo* make **34** a suitable tool for probing the potential of DYRK1A/1B inhibition in various disease models, keeping in mind potential interference from inhibition of the CLK family at high concentrations. In the study reported here, the *in vivo* efficacy was assessed in a human xenograft tumor model.

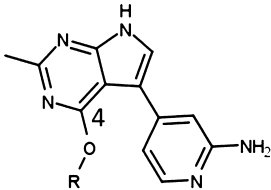
Previous work has demonstrated that glioblastoma cells are dependent on DYRK1A for growth, both *in vitro* and *in vivo*.¹⁵ Compound **34** inhibited the proliferation of U87MG glioblastoma cells grown either as a 2D monolayer (Figure S4A) or as multicellular tumor spheroids (Figure S4B). Activity was dependent on serum concentration with increased activity observed under lower serum conditions. **34** was administered po at 25, 100, and 200 mg/kg to female nude mice bearing established U87MG tumors and tumor concentration measured at 6 and 16 h (Figure 3C) post dose. Good plasma and tumor exposure were observed following either a 100 or 200 mg/kg oral dose with compound levels in the tumor above that needed to inhibit U87MG cell growth *in vitro* for at least 16 h following the administration of the highest dose. It was not possible to measure the DYRK1A biomarker (pS520 phosphorylation) due to the low level of expression in these cells. Further work is ongoing to identify novel biomarkers of DYRK1A inhibition. As shown in Figure 6A, **34** significantly inhibited the proliferation of established U87MG xenografts with tumor growth delays (TGDs) of 93% ($P < 0.01$) and 224% ($P < 0.001$) following daily oral administration of 100 and 200 mg/kg, respectively. Little to no toxicity was observed at these doses (Figure 6B).

Comparison of the Binding of **34 with Other Recently Published DYRK1A Inhibitors.** A number of recent studies have generated crystal structures of other series of inhibitors of DYRK1A, derived from natural products such as the leucettines⁴⁴ and harmine^{41,45} or from profiling⁴⁶ or elaboration⁴⁷ of known kinase binding motifs and fragment molecules.⁴⁸ Figure 7 shows the chemical structures of representatives of these chemical series and **34**, oriented approximately as they bind in Dyrk1a and highlighting various features, in particular, the interactions with amino acids in the kinase hinge and with K188. The binding pose as seen in the crystal structures for these compounds is shown in Figure S5.

The most similar hinge-binding heterocycle to the pyrrolopyrimidine of **34** is the pyrrolopyridine of 6EIF⁴⁶ (**38**) and 6S1H (**39**) with two of the heterocyclic nitrogens of the amino-pyrimidine in 6EIL (**45**) making the same hydrogen bonds. Similarly, 6QU2 (**40**) has a pyrimidine as part of a tricycle in an equivalent position as that in **34** with a cyclopropyl group occupying the position of the methyl. A number of methyl amino pyrimidines such as 6S1H (**39**) position the methyl in the same position but with different

Table 4. Selectivity in a Small Assay Panel of Protein Kinases (IC₅₀ μ M)

compd no	ADP DYRK1A	TR FRET DYRK1A	TR FRET DYRK1B	ADP DYRK2	TR FRET CDK9	ADP PAK4	ADP Pim1	ADP Aurora A
18	0.05					>50	>50	>50
19	0.02	0.02	0.02	0.06	4.4	>50	2.8	>50
20	0.04	0.03	0.04	0.30	>10	>50	9.6	>50

Table 5. SAR and Selectivity of O-Linked Aryls at 4-Position of the Pyrimidine Ring (IC_{50} μM)


Example	19	24	25	26	27	28
R1	Me					
ADP DYRK1A	0.023	0.006	0.011	0.011	0.012	0.012
ADP Pim1	2.8	0.079	>50	0.489	0.36	>50
ADP TTK	-	-	0.10	-	0.099	-
TR Fret DYRK1A	0.018	0.009	0.015	-	0.015	0.017
TR Fret DYRK1B	0.022	0.001	0.018	-	0.001	0.013
TR Fret DYRK2	0.065	0.008	0.40	-	0.002	0.40
TR Fret CLK	-	0.017	0.033	-	0.024	-
TR Fret CDK9	4.4	1.9	>10	-	>10	>10

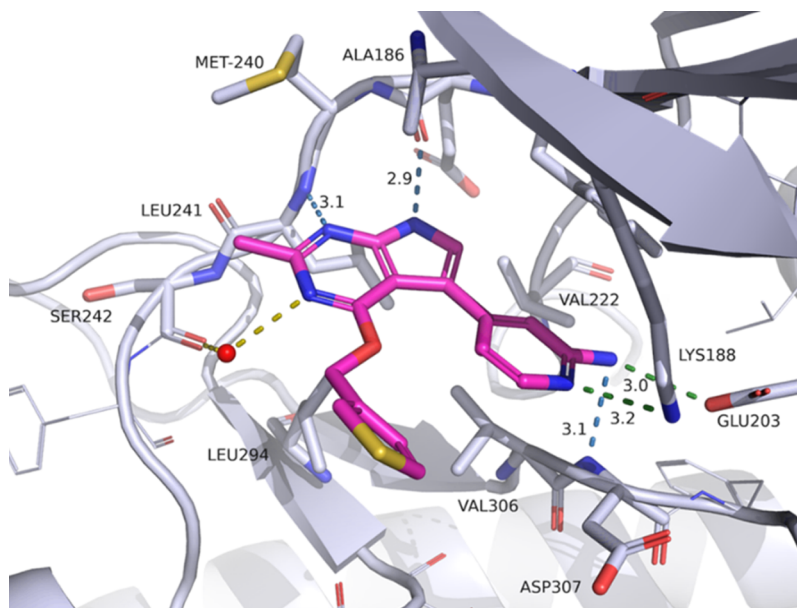
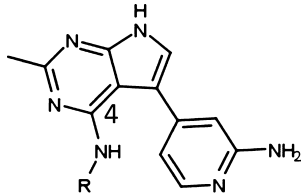
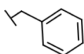
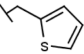
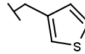
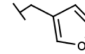
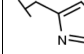


Figure 4. Structure of 24 bound to Dyrk1a (PDB: 7A5L). See the legend to Figure 1 for conventions used in the representation.

positions and orientations of the pyrimidine. There are a large number of other structures where atoms or small groups fill the “methyl” hole—some of which are derived from natural compounds such as harmine as in 3ANR (9) and leucettine as in 4AZE (42) and others where a methoxy benzene on benzothiazole, as in 5A4L (43), or halogen in the methyl position, such as Br in 4YLL (44).

The interaction made with K188 through compound optimization (as seen in Figures 3 and 4) is a common feature of many DYRK1A inhibitors such as the equivalent pyridine ring in 6EIF (38) and 6QU2 (40), although just past the conventional limit of hydrogen bonding distance (3.5 Å) for 34 and for 6EIL (45). There are, however, no published structures where the substituents mimic the full extent of the

Table 6. SAR and Selectivity of Aryls at 4-Amino Position (IC₅₀ μM)


Example	29	30	31	32	33
R					
ADP DYRK1A	0.015	0.025	0.027	0.043	0.051
ADP Pim1	4.1	3.7	4.2	6.2	13.6
Radiometric Gsk3β	>10	>10	>10	>10	-
TR FRET DYRK1A	0.006	0.007	0.009	0.025	-
TR FRET DYRK1B	0.001	0.001	0.006	0.009	-
ADP DYRK2	0.15	0.014	0.093	0.21	-
TR FRET CDK9	>10	>10	5.5	>10	-

interactions made by the difluorobenzene substituent in **34** that sits within a hydrophobic region. The only compound for which a substructure reaches the same pocket is the iodine substituent of **4YLL** (**44**); however, this does not fully occupy the available space. One interesting comparison is between the pose for **41** and that for **39**—the change from a pyrrolo-pyridine (**41**) to a pyrazolo-pyridazine (**39**) leads to a flip of the binding mode, presumably because of changed hydrogen bonding potential.

CHEMISTRY

Compounds **11**–**17** shown in Table 2 introduced aryls and heteroaryls into the 6-position, and these were prepared in an analogous manner to **16** (Scheme 1).

16 was prepared starting from commercially available 1,1,2,2-ethenetetracarboxitrile and cyclization to form the amino pyrrole **38** using HBr in acetic acid (Scheme 1). Ring closure to form the pyrimidine ring was performed using triethyl orthoacetate under refluxing conditions followed by methanolic ammonia in a sealed vessel to isolate key intermediate **39**. The 6-position bromo facilitated in installation of aromatics and heteroaromatics such as the 3-pyridinyl moiety via a Suzuki coupling to form compound **16**.

To investigate different substituents at the 4-position, we prepared a series of 4-alkoxy compounds (Table 3). These were prepared via a similar route to **19**, as outlined in Scheme 2. Starting from commercially available 4-chloro-2-methyl-7H-pyrrolo[2,3-d]pyrimidine, the pyrrole-7H was first protected with a SEM group and then brominated at the 5-position using *N*-bromosuccinamide. The formation of the appropriate alkoxide with sodium hydride and S_NAr to substitute the 4-chloro occurs. The 5-position pyridines were installed via Suzuki coupling and finally deprotection of the SEM using tetrabutyl ammonium fluoride solution.

In a similar manner, we used the appropriate primary amines to install 4-aminoaryls such as **34** of which the preparation is outlined in Scheme 3, using triethylamine as a tertiary base. Compounds shown in Table 6 were prepared via a similar route, starting with the SEM-protected intermediate **19a**.

In order to investigate pyrimidines at the 5-position, we needed to change the protection and deprotection strategy for the pyrrole ring 7 N. To prepare **35**, we first installed the benzene sulfonyl-protecting group and reversed the coupling partners to install the 5-position aminopyridine. This route involved the preparation of the intermediate 5-boronate ester (**50**) prior to the Suzuki coupling with amino-4-chloropyrimidine, as shown in Scheme 4.

To investigate 4-aryl substituents, we again modified the 7 N protection strategy employing boc-protection after installation of the 4 aryls via Suzuki coupling. We found that bromination in the 5-position and protection of the 7 N with boc-anhydride could be performed in a single step isolating the intermediate **53** by purification, as shown in Scheme 5. A second Suzuki coupling under conditions similar to previous examples installed the 5-position aminopyridine moiety.

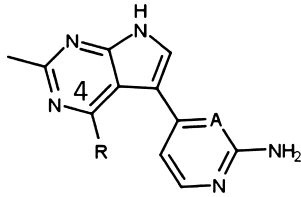
All tested compounds were of >95% purity (NMR spectra for **34** and MS traces for **34**–**37** in the Supporting Information).

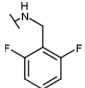
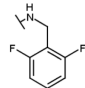
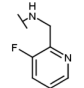
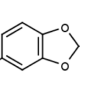
CONCLUSIONS

We have used fragment and structure-based discovery methods to identify **34**, a potent, *in vivo*-tolerated, selective inhibitor of DYRK1A kinase.

The methyl group on the pyrrolopyrimidine of **34** is an important determinant of selectivity for DYRK1A against other kinases, as it occupies a small hydrophobic pocket adjacent to Leu 244 for which the carbonyl of the backbone peptide bond has a different orientation to that seen in most protein kinases. As shown in Figure 7, the introduction of other hydrophobic

Table 7. Investigation of the SAR and Cellular Activity of Aryls at the 4-Position



Example	34	35	36	37
A	C	N	C	C
R				
IC ₅₀ (μM)				
ADP DYRK1A	0.007	0.008	0.008	0.01
ADP DYRK2	0.08	0.05	0.03	>10
TR-FRET DYRK1A	0.004	0.01	0.005	0.003
TR-FRET DYRK1B	0.003	0.01	0.007	0.01
TR-FRET DYRK2	0.25	0.02	0.02	1.8
TR-FRET DYRK3	0.14	-	0.03	-
TR-FRET DYRK4	3.0	-	1.6	-
TR-FRET CLK1	0.02	0.02	0.02	0.04
TR-FRET CDK9	>10	>10	>10	>10
CELL U2OS pS520	0.02	0.001	0.03	0.04
Caco2 permeability (Papp cm s ⁻¹)	4.4	21	0.9	6.5
Liver microsome stability - M/R/H (ml/min/kg), %HBF	124/74 /15 83/92/68	100/53/18 67/66/84	100/53/13 66/67/60	89/50/12 60/62/58
hERG % inhibition at (1 / 3 / 10) μM	28/72/79	25/42/59	21/41/54	66 at 10 μM

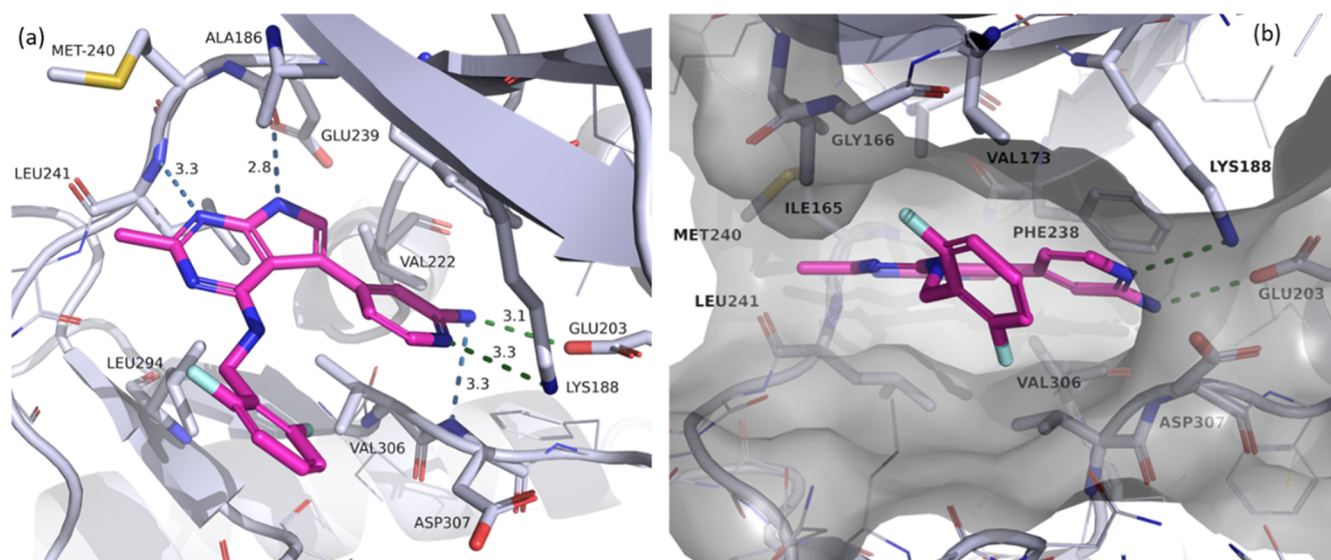


Figure 5. Structure of **34** (PDB code: 7A5N) bound to Dyk1a. (a) See the legend in Figure 1 for conventions used in the representation. (b). Alternate view to show hydrophobic interactions with underside of the glycine loop.

groups in this region is a feature of other DYRK1A inhibitors identified elsewhere. However, other features of **34** are distinctive. The difluoro-benzene moiety is in a portion of the active site of Dyk1a not occupied by compounds in other published structures; similarly, the amino group on the

pyridine moiety makes a hydrogen bond not mirrored by other compounds for which structures are available. Although **34** has similar potency to an inhibitor of DYRK1A and DYRK1B enzymes, it is highly selective against most other kinases; one of the exceptions is CLK1 for which a crystal

Table 8. Mean Plasma Concentration \pm SD in ng/mL of 34 Measured after po Administration (Three Animals/Time Point)

	0.5 h	2h	6h	16h
25 mpk	850 \pm 246	1828 \pm 805	451 \pm 503	
100 mpk		12176 \pm 7809	15177 \pm 2430	322 \pm 503

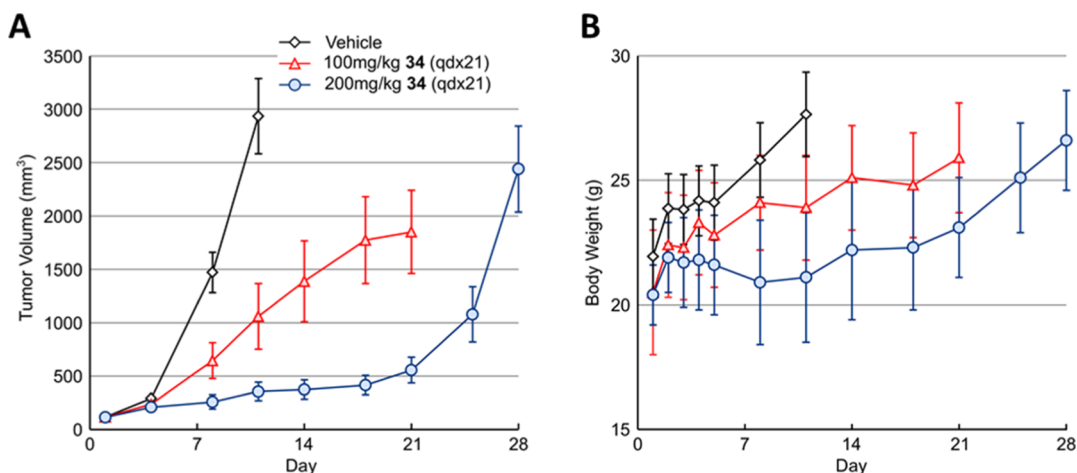


Figure 6. Compound 34 inhibits the growth of U87MG glioblastoma xenografts. Nude mice with established U87MG subcutaneous tumor xenografts were dosed with either 100 or 200 mg/kg PO 34 daily for 21 days (qdx21). Tumor volume (A) was determined by twice weekly caliper measurement, and body weight (B) was recorded.

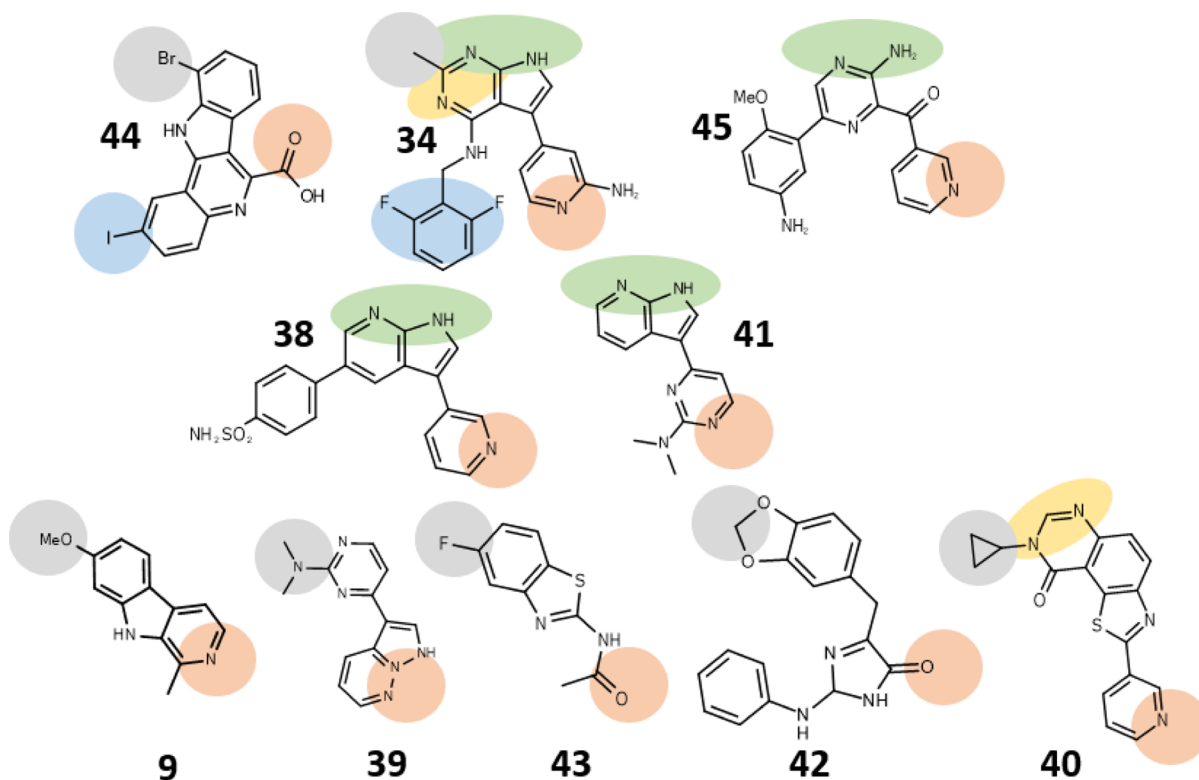
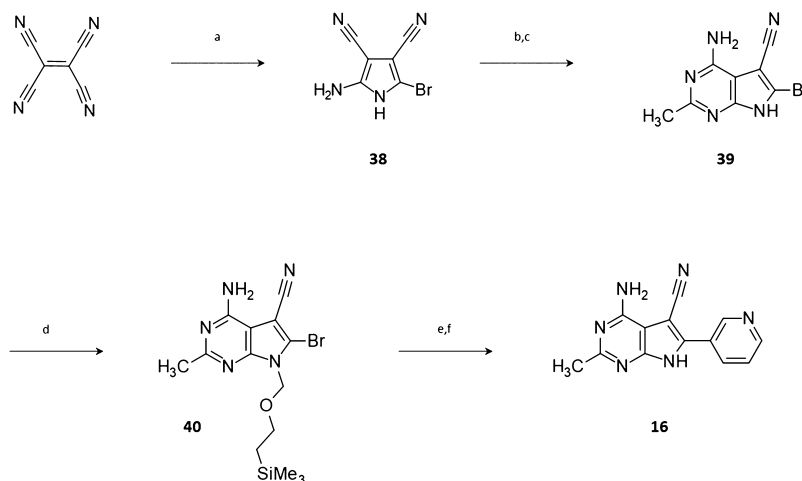


Figure 7. 34 and representatives of different classes of DYRK1A inhibitors drawn in approximately the relative orientation seen in the available crystal structures for binding to Dyrk1a. Shading highlights equivalent features: green—equivalent to pyrrolopyrimidine hinge binding; gray—equivalent to the methyl of 34, binding in the small hydrophobic pocket adjacent to carbonyl of L241; yellow—equivalent pyrimidine; blue—equivalent interactions to the hydrophobic pocket; and pink—interaction with K188. See the text for references.

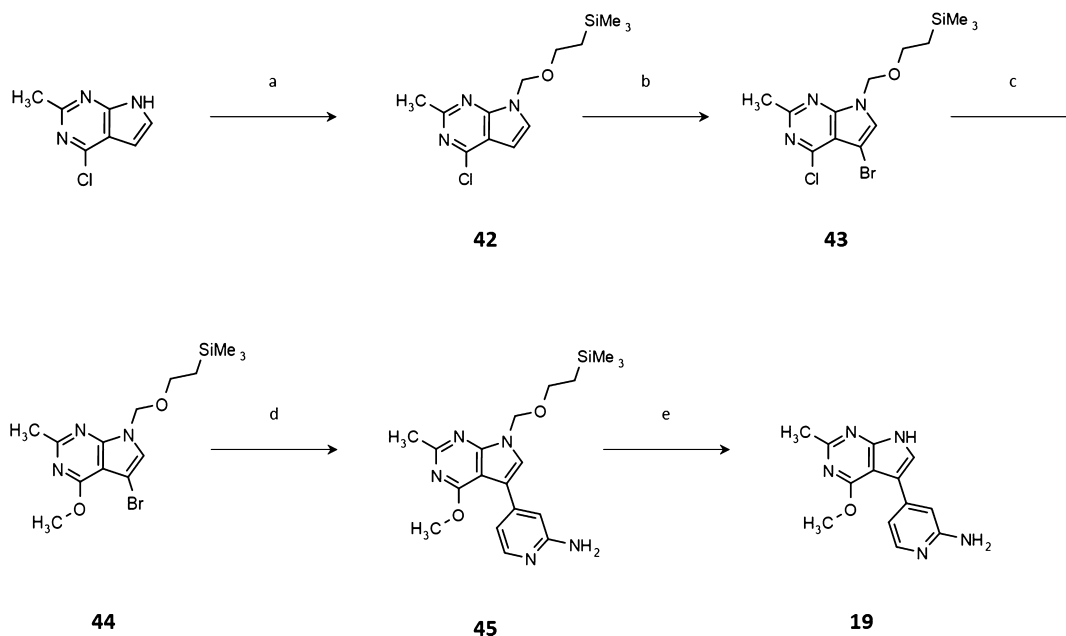
structure demonstrates a similar hydrophobic pocket in the kinase hinge due to a similar peptide conformation in the kinase hinge to that seen in Dyrk1a.

34 has many of the properties desired for a tool compound to probe the biological effects of DYRK1A inhibition. *In vitro*,

it demonstrates potent inhibition of DYRK1A with concomitant target engagement in cells. It is orally bioavailable and tolerated at doses over 100 mg/kg and achieves sufficient plasma and tumor exposure to show efficacy in an *in vivo* model of glioblastoma with a PD marker (phosphorylation of

Scheme 1. Preparation of Compound 16^a

^aReagents and conditions: (a) 33% HBr in acetic acid, acetone, -10 to -5 °C, 3 h; (b) triethyl orthoacetate, MeCN, reflux, yield 63%; (c) 7 N NH_3 in MeOH, sealed vessel, 105 °C, 6 h, yield 59%; (d) NaH, SEM-Cl, DMF, yield 57%, yield 48%; (e) pyridine-3-boronic acid, K_2CO_3 , THF, water [1,1'-Bis(diphenylphosphino)ferrocene]dichloropalladium(II) (10 mol %), 130 °C; and (f) ethylenediamine, TBAF (1 M in THF), 120 °C microwave, 30 min, yield 38%.

Scheme 2. Synthesis of 19^a

^aReagents and conditions: (a) SEM-Cl, NaH, DMF, 0 °C, 2 h, yield quant; (b) NBS, DMF, rt, yield 72%; (c) NaH, MeOH, 0 °C, yield quant; (d) (2-aminopyridin-4-yl)boronic acid, THF, water, K_2CO_3 , cat [1,1'-Bis(diphenylphosphino)ferrocene]dichloropalladium(II), 1 h microwave, 140 °C, yield 32%; and (e) TBAF (1 M in THF), ethylenediamine, THF, yield 43%.

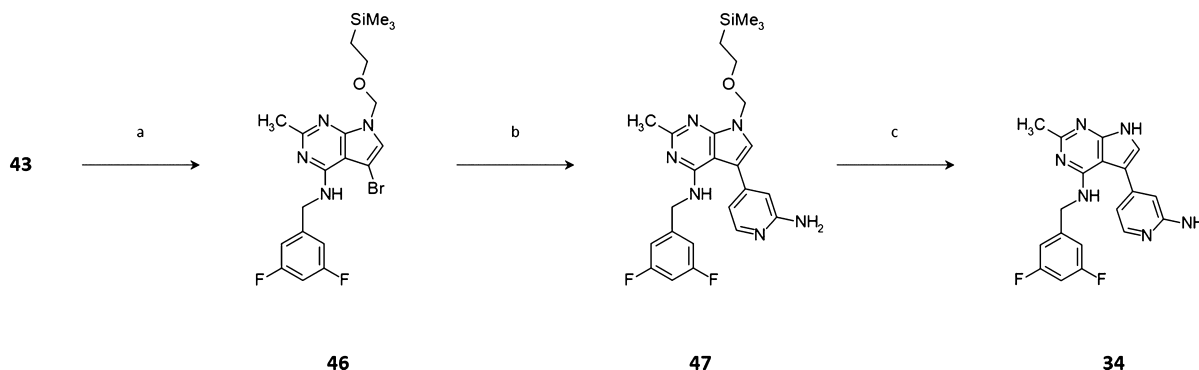
S520), confirming cellular target engagement. This compound will be a useful tool to explore further the functional consequence of DYRK1A inhibition which may lead to new therapeutic strategies in oncology and Down's syndrome.

EXPERIMENTAL SECTION

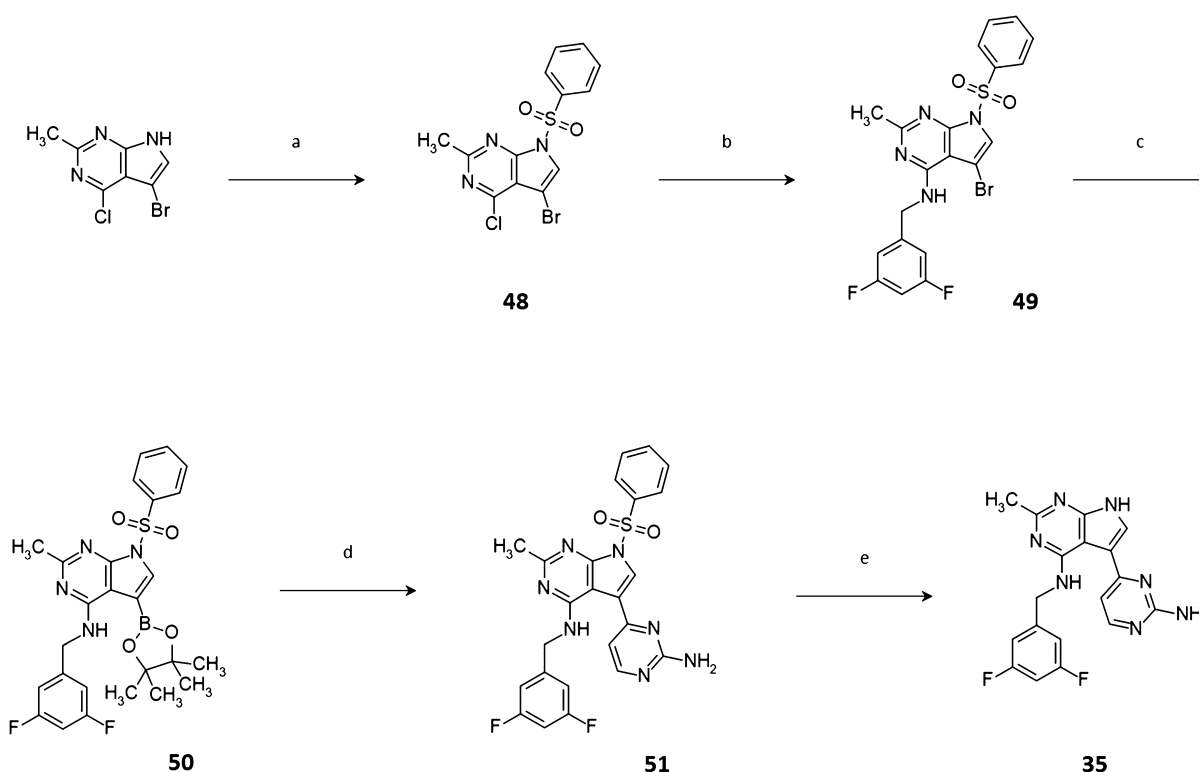
All chemicals were used directly as received from commercial suppliers. ^1H spectra were recorded on AVANCE III HD 400 (400 MHz for ^1H , BRUKER). Chemical shifts for ^1H are reported in parts per million (ppm) referenced to the residual solvent peak ($\text{DMSO}-d_6$, $\delta = 2.50$ ppm). Abbreviations used to describe the peak signals in ^1H NMR data are s = singlet, br = broad, d = doublet, dd = double doublet, dt = double triplet, t = triplet, td = triple doublet, tt = triple

triplet, q = quartet, quin = quintet, and m = multiplet. All compounds were determined as having purity >95% unless stated otherwise, and all final tested compounds were purified to >95% by reverse-phase high-performance liquid chromatography (HPLC), or normal-phase silica gel column chromatography. The purity was assessed by reverse-phase ultraperformance liquid chromatography with a gradient of 5–98% acetonitrile in water (with either the acid or base modifier) and monitored by UV absorption at 210–450 nm.

Unless otherwise described, the following conditions were used for compound synthesis, purification, and analysis. A CEM microwave was used for the microwave reaction conditions. OH-type silica gel column chromatography was performed using ISCO Combi-flash RF or RF Gold. The prep-HPLC purifications were performed using

Scheme 3. Synthesis of 34^a

^aReagents and conditions: (a) 2,6-difluorobenzylamine, TEA, EtOH, 80 °C, 16 h, yield 87%; (b) 2-aminopyridine-4-boronic acid pinacol ester, K₂CO₃, Pd-118 (cat), THF, water, 60 °C, 16 h, yield: 76%; and (c) TBAF (1 M in THF) ethylenediamine, THF, 80 °C, 14 h, yield 59%.

Scheme 4. Synthesis of 35^a

^aReagents and conditions: (a) benzene sulfonyl chloride, NaH, DMF, 0 °C, 16 h, yield 91%; (b) 2,6-difluorobenzylamine, TEA, ethanol, 80 °C, 16 h, yield 93%; (c) bis(pinacolato)diboron, KOAc, PdCl₂(PPh₃)₂, THF, 140 °C, 1 h, yield 61%; (d) 2-amino-4-chloropyrimidine, K₂CO₃, Pd118, THF, 90 °C, 2 h, yield 64%; and (e) K₂CO₃, methanol, RT, 16 h, yield 40%.

Waters prep LCMS [ionization method: electron spray ionization (ESI)].

The following compounds 11–15 were prepared in an analogous manner to compound 16.

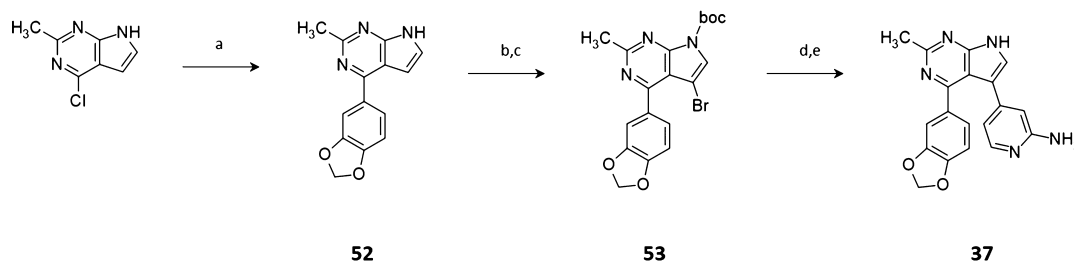
4-Amino-7-ethyl-2-methyl-6-(pyridine-3-yl)-7H-pyrrolo[2,3-d]pyrimidine-5-carbonitrile (11). It was isolated as a colorless solid, 32 mg (0.11 mmol) (yield 7%). ¹H NMR (400 MHz, DMSO-*d*₆): δ 8.89–8.78 (m, 2H), 8.14 (m, 1H), 7.73–7.58 (m, 2H), 6.84 (s, 2H), 4.17 (q, *J* = 7.16 Hz, 2H), 2.47 (s, 3H), 1.15 (t, *J* = 7.16 Hz, 3H). MS (ESI⁺) *m/z*: 279[M + H]⁺. HRMS (ESI⁺/APCI): calcd for [C₁₅H₁₄N₆+H]⁺, 279.1284; found, 279.1356.

4-Amino-6-(2,3-difluorophenyl)-7-ethyl-2-methyl-7H-pyrrolo[2,3-d]pyrimidine-5-carbonitrile (12). It was isolated as a colorless solid, 15 mg (0.05 mmol) (yield 3%). ¹H NMR (400 MHz, DMSO-*d*₆): δ 7.83–7.71 (m, 1H), 7.58–7.45 (m, 2H), 6.88 (s, 2H),

4.10 (q, *J* = 7.14 Hz, 2H), 2.47 (s, 3H), 1.15 (t, *J* = 7.15 Hz, 3H). MS (ESI⁺) *m/z*: 314[M + H]⁺. HRMS (ESI⁺/APCI): calcd for [C₁₆H₁₃N₅F₂+H]⁺, 314.1139; found, 314.1217.

4-Amino-6-(2,3-difluorophenyl)-7-methyl-2-methyl-7H-pyrrolo[2,3-d]pyrimidine-5-carbonitrile (13). It was isolated as a colorless solid, 18 mg (0.06 mmol) (yield 32%). ¹H NMR (400 MHz, DMSO-*d*₆): δ 7.82–7.70 (m, 1H), 7.59–7.44 (m, 2H), 6.89 (s, 2H), 3.61 (d, *J* = 0.97 Hz, 3H), 2.46 (s, 3H). MS (ESI⁺) *m/z*: 300[M + H]⁺. HRMS (ESI⁺/APCI): calcd for [C₁₅H₁₁N₅F₂+H]⁺, 300.0983; found, 300.1059.

4-Amino-6-(5-methoxypyridin-3-yl)-2,7-dimethyl-7H-pyrrolo[2,3-d]pyrimidine-5-carbonitrile (14). It was isolated as a colorless solid, 28 mg (0.10 mmol) (yield 13%). ¹H NMR (400 MHz, DMSO-*d*₆): δ 8.52 (d, *J* = 2.9 Hz, 1H), 8.47 (d, *J* = 1.8 Hz, 1H), 7.76 (dd, *J* = 2.9, 1.8 Hz, 1H), 3.93 (s, 3H), 3.69 (s, 3H), 3.35 (s, 2H),

Scheme 5. Synthesis of 37^a

^aReagents and conditions: (a) 3,4-(methylenedioxy)-phenyl boronic acid, Cs₂CO₃, palladium(dppf)Cl₂, THF, water, 130 °C, 45 min, yield quant; (b) NBS, DMF 0 °C, 2 h, yield 54%; (c) boc-anhydride, DMAP, Et₃N; (d), boc-2-aminopyridine-4-boronic acid pinacol ester, K₂CO₃, Pd118, THF, water, 65 °C, 16 h; and (e) HCl in MeOH, microwave 90 °C, 1 h, yield 27% (over two steps).

2.47 (s, 3H). MS (ESI⁺) *m/z*: 295[M + H]⁺. HRMS (ESI⁺/APCI): calcd for [C₁₅H₁₄N₆O + H]⁺, 295.1229; found, 295.1307.

4-Amino-2,7-dimethyl-6-(pyridine-3-yl)-7H-pyrrolo[2,3-d]pyrimidine-5-carbonitrile (15). It was isolated as a colorless solid, 28 mg (0.11 mmol) (yield 28%). ¹H NMR (400 MHz, DMSO): δ 8.90 (dd, *J* = 2.3, 0.9 Hz, 1H), 8.80 (dd, *J* = 4.9, 1.6 Hz, 1H), 8.17 (dd, *J* = 2.4, 1.7 Hz, 1H), 7.68 (dd, *J* = 4.9, 0.9 Hz, 1H), 6.84 (s, 2H), 3.68 (s, 3H), 2.47 (s, 3H). MS (ESI⁺) *m/z*: 265[M + H]⁺. HRMS (ESI⁺/APCI): calcd for [C₁₄H₁₂N₆+H]⁺, 265.1123; found, 265.1199.

4-Amino-2-methyl-6-(pyridine-3-yl)-7H-pyrrolo[2,3-d]pyrimidine-5-carbonitrile (16). **Step 1.** 2-Amino-5-bromo-1H-pyrrole-3,4-dicarbonitrile (**38**). A 3 L flask was fitted with a condenser, a drying tube, and an internal thermometer. The flask was cooled in a methanol/ice bath. Ethyl acetate (1 L), acetone (185 mL), and 1,1,2,2-ethenetetracarboxitrile, Sigma-Aldrich T8809 (50 g, 0.39 mol), were added. The solution was cooled to −10 °C (methanol/ice bath), and HBr (287 mL, 33% in acetic acid solution, 3 equiv) was added dropwise at such a rate as to maintain −5 °C (over ~1 h). A yellow solid began to precipitate during the addition. After the addition was complete, the suspension was stirred for an additional 3 h. The yellow precipitate was collected by filtration and washed with ethyl acetate (2 × 100 mL) and diethyl ether (2 × 100 mL). The solid cake was then suspended in water (600 mL), and the pH was adjusted to 11 with 50% NaOH, giving a dark solution. Decolorizing charcoal (ca. 15 g) was then added to the solution and filtered through celite, and the filtrate was acidified to pH 5 with glacial acetic acid. The mixture was allowed to stand at rt overnight. The product was then collected by filtration and dried at 40 °C in a vacuum oven for 5 days to give the title compound as a brown solid, 52 g (yield 63%). ¹H NMR (400 MHz, DMSO-*d*₆): δ 12.33 (s, 1H), 6.49 (s, 2H).

4-Amino-6-bromo-2-methyl-7H-pyrrolo[2,3-d]pyrimidine-5-carbonitrile (39). **38** (8.44 g, 40 mmol) was suspended in dry acetonitrile (150 mL). Triethyl orthoacetate (11 mL, 60 mmol, 1.5 equiv) was added, and the mixture was heated at rt for ~1 h. The dark brown solution was cooled to rt and filtered through a filter paper. Acetonitrile was removed under vacuum to afford a brown solid which was transferred to a steel reaction vessel. 7 N NH₃ in MeOH (200 mL) was added, and the vessel was then sealed and heated to 105 °C for 6 h. The vessel was cooled to rt overnight, and the resulting solid was collected by filtration. The crude solid was washed several times with methanol followed by diethyl ether to furnish the title compound as a gray solid, 6 g (yield 59%). ¹H NMR (400 MHz, DMSO-*d*₆): δ 13.81 (s, 1H), 7.34 (s, 2H), 2.43 (s, 3H). MS (ESI⁺) *m/z*: 254[M + H]⁺.

4-Amino-6-bromo-2-methyl-7-²³-7H-pyrrolo[2,3-d]pyrimidine-5-carbonitrile (40). To a suspension of **39** (200 mg, 0.8 mmol) in dry dimethylformamide (DMF) (10 mL) was added sodium hydride (60% in mineral oil (32 mg, 0.8 mmol, 1 equiv) at rt). The suspension became a dark clear solution after ca. 5 min. The mixture was stirred for 30 min before adding SEM-Cl (140 μL, 0.8 mmol, 1 equiv) at rt and stirred under nitrogen for 2 h. The reaction mixture was diluted with ethyl acetate (50 mL), washed with brine (2 × 50 mL), dried over anhydrous magnesium sulfate, and concentrated under vacuum.

Purification was performed by flash column chromatography to furnish the title compound as a mixture of regio-isomers (ratio ~1:1), 172 mg (yield 57%). MS (ESI⁺) *m/z*: 384[M + H]⁺ (2 overlapping peaks, isomers seen by LCMS).

4-Amino-2-methyl-6-(pyridine-3-yl)-7-[[2-(trimethylsilyl)ethoxy]-methyl]-7H-pyrrolo[2,3-d]pyrimidine-5-carbonitrile (41). **40** (100 mg, 0.26 mmol) and pyridine-3-boronic acid (48 mg, 0.39 mmol, 1.5 equiv) were dissolved in a mixture of THF/water (5:1, 6 mL) under nitrogen. The mixture was treated with potassium carbonate (311 mg, 0.52 mmol, 2 equiv), and [1,1-bis(diphenylphosphino)ferrocene]-dichloropalladium(II) (19 mg, 10 mol %) was added, and the resulting mixture was degassed with a stream of nitrogen for 5 min. The reaction mixture was heated at 130 °C in a CEM microwave for 60 min. The whole mixture was then diluted with dichloromethane (20 mL), and water was added (20 mL). The organic layer was separated, washed with brine, dried over magnesium sulfate, and concentrated under vacuum. The crude residue was purified using flash column chromatography to furnish the title compound as a yellow solid, 48 mg (yield 48%). MS (ESI⁺) *m/z*: 381[M + H]⁺.

4-Amino-2-methyl-6-(pyridine-3-yl)-7H-pyrrolo[2,3-d]pyrimidine-5-carbonitrile (16). To a solution of 3001-AF-085 4-amino-2-methyl-6-(pyridine-3-yl)-7-[[2-(trimethylsilyl)ethoxy]-methyl]-7H-pyrrolo[2,3-d]pyrimidine-5-carbonitrile (48 mg, 0.13 mmol) in tetrahydrofuran (THF) (3 mL) was added ethylenediamine (42 μL, 0.63 mmol, 5 equiv) followed by TBAF (1 M solution in THF) (0.63 mL, 0.63 mmol, 5 equiv). The reaction was heated to 120 °C for 30 min in a microwave. The reaction mixture was poured into a mixture of water and ethyl acetate (10 mL, 1:1) and stirred for ~15 min. The aqueous layer was separated and concentrated under vacuum. The resulting precipitate was triturated in acetonitrile, and the solid was collected by filtration. The solid was washed lightly with diethyl ether and dried under vacuum to give the title compound as a colorless solid, 12 mg (yield 38%). ¹H NMR (400 MHz, DMSO-*d*₆): δ 13.02 (s, 1H), 9.11 (d, *J* = 2.3 Hz, 1H), 8.70 (dd, *J* = 4.8, 1.6 Hz, 1H), 8.29 (dt, *J* = 8.1, 2.0 Hz, 1H), 7.64 (dd, *J* = 8.0, 4.7 Hz, 1H), 6.79 (s, 2H), 2.43 (s, 3H). MS (ESI⁺) *m/z*: 251[M + H]⁺. HRMS (ESI⁺/APCI): calcd for [C₁₃H₁₀N₆+H]⁺, 251.0967; found, 251.1042.

4-Amino-6-(2,3-difluorophenyl)-2-methyl-7H-pyrrolo[2,3-d]pyrimidine-5-carbonitrile (17). Compound **17** was prepared in an analogous manner to compound **16**. The title compound was isolated as a colorless solid, 10 mg (0.03 mmol) (yield 31%). ¹H NMR (400 MHz, DMSO-*d*₆): δ 13.04 (s, 1H), 7.66 (q, *J* = 8.7 Hz, 1H), 7.61–7.52 (m, 1H), 7.45 (q, *J* = 5.4, 3.4 Hz, 1H), 6.81 (s, 2H), 2.43 (s, 3H). MS (ESI⁺) *m/z*: 286[M + H]⁺. HRMS (ESI⁺/APCI): calcd for [C₁₄H₉N₅F₂+H]⁺, 286.0826; found, 286.0902.

4-[4-Methoxy-2-methyl-7H-pyrrolo[2,3-d]pyrimidin-5-yl]pyridine (18). 4-[4-methoxy-2-methyl-7H-pyrrolo[2,3-d]pyrimidin-5-yl]pyridine (**18**) was as prepared in an analogous manner to compound **19**. The title compound was isolated as a colorless solid, 15 mg (yield 21%). ¹H NMR (400 MHz, DMSO-*d*₆): δ 12.33 (s, 1H), 8.58–8.50 (m, 2H), 7.85 (s, 1H), 7.78–7.72 (m, 2H), 4.05 (s, 3H), 2.57 (s, 3H). MS (ESI⁺) *m/z*: 241[M + H]⁺. HRMS (ESI⁺/APCI): calcd for [C₁₃H₁₂N₄O + H]⁺, 241.1011; found, 241.1082.

4-[4-Methoxy-2-methyl-7H-pyrrolo[2,3-d]pyrimidin-5-yl]pyridine-2-amine (19). **Step 1.** 4-Chloro-2-methyl-7-[[2-(trimethylsilyl)ethoxy]methyl]-7H-pyrrolo[2,3-d]pyrimidine (**42**). To a solution of 4-chloro-2-methyl-7H-pyrrolo[2,3-d]pyrimidine (Combi-Blocks ST-3008) (1.85 g, 11 mmol) in dry DMF (30 mL) was added sodium hydride (60% in mineral oil) (290 mg, 12 mmol) at 0 °C under nitrogen. The mixture was stirred for 30 min before adding SEM-Cl (2.34 mL, 13 mmol 1.2 equiv) dropwise at 0 °C, and after addition, the whole mixture was stirred under nitrogen for 2 h. The reaction mixture was diluted with diethyl ether (100 mL), washed with brine (2 × 50 mL), dried over anhydrous magnesium sulfate, and concentrated under vacuum to give the title compound as brown oil, 3.57 g (yield quant) (purity determined by LCMS 90%). The crude product title compound was used in the subsequent step without further purification. MS (ESI⁺) *m/z*: 298 [M + H]⁺.

5-Bromo-4-chloro-2-methyl-7-[[2-(trimethylsilyl)ethoxy]methyl]-7H-pyrrolo[2,3-d]pyrimidine (43). To a solution of crude **42** (3.3 g, 11 mmol) in DMF (30 mL) was added *N*-bromosuccinamide (2 g, 11 mmol, 1 equiv) in DMF (5 mL) at 0 °C under N₂. It was stirred for 30 min at 0 °C and then allowed to warm to rt over 30 min. The reaction mixture was diluted with water (20 mL) and extracted with diethyl ether (30 mL). The organic layer was washed several times with water, dried over anhydrous magnesium sulfate, and concentrated in vacuum. The residue was purified by flash column chromatography to give the title compound as a colorless solid, 3 g (yield 72% over two steps). ¹H NMR (400 MHz, DMSO-*d*₆): δ 8.13 (s, 1H), 5.65 (s, 2H), 3.66–3.57 (m, 2H), 2.74 (s, 3H), 0.98–0.88 (m, 2H). MS (ESI⁺) *m/z*: 378 [M + H]⁺.

5-Bromo-4-methoxy-2-methyl-7-[[2-(trimethylsilyl)ethoxy]methyl]-7H-pyrrolo[2,3-d]pyrimidine (44). To a suspension of sodium hydride (60% suspension in mineral oil) (530 mg, 13 mmol, 2 equiv) in THF (10 mL) was added methanol (346 μL, 8.6 mmol, 1.3 equiv) dropwise at 0 °C (ice bath cooling). The mixture was stirred for approximately 10 min before adding **43** (2.5 g, 6.6 mmol) in THF (10 mL) under N₂ at 0 °C. The reaction mixture was stirred at 0 °C for 30 min and allowed to warm to rt over 1 h. The reaction was quenched with saturated NH₄Cl(aq) (50 mL) and extracted with ethyl acetate (50 mL). The organic layer was washed with brine, dried over anhydrous magnesium sulfate, and concentrated under vacuum to give the title compound as light yellow oil (2.4 g, yield quant). MS (ESI⁺) *m/z*: 372 [M + H]⁺.

4-[4-Methoxy-2-methyl-7-[[2-(trimethylsilyl)ethoxy]methyl]-7H-pyrrolo[2,3-d]pyrimidin-5-yl]pyridine-2-amine (45). **44** (150 mg, 0.4 mmol) and (2-aminopyridin-4-yl)boronic acid (133 mg, 0.6 mmol, 1.5 equiv) were dissolved in a mixture of THF and water (6:1, 5 mL) under nitrogen. Potassium carbonate (166 mg, 1.2 mmol, 3 equiv) and [1,1'-bis(diphenylphosphino)ferrocene]dichloropalladium(II) (15 mg, 5 mol %) were added, and the resulting mixture was degassed with a stream of N₂ for 5 min. The reaction mixture was heated at 140 °C in a CEM microwave for 1 h. The product mixture was diluted with water (10 mL) and extracted with ethyl acetate. The organic layer was washed with brine, dried over anhydrous magnesium sulfate, and concentrated under vacuum. The resulting crude product oil was taken up in dichloromethane and dry-loaded onto ISOLUTE before purification by flash column chromatography to afford the title compound as a colorless solid, 50 mg (yield 32%). MS (ESI⁺) *m/z*: 386 [M + H]⁺.

4-[4-Methoxy-2-methyl-7H-pyrrolo[2,3-d]pyrimidin-5-yl]pyridine-2-amine (19). To a solution of **45** (50 mg, 0.13 mmol) in THF (3 mL) was added ethylenediamine (43 μL 0.65 mmol, 5 equiv) followed by TBAF (1 M in THF, 5 equiv). The reaction was stirred at 80 °C for 2 h in the microwave. The reaction mixture was poured into water and ethyl acetate (20 mL, 1:1) and stirred for 15 min. The organic layer was separated, washed with brine, dried over anhydrous magnesium sulfate, and concentrated under vacuum. The residue was then triturated with acetonitrile and collected by filtration to furnish the title compound as a colorless solid, 15 mg (yield 43%). ¹H NMR (400 MHz, DMSO-*d*₆): δ 12.16 (s, 1H), 7.86 (dd, *J* = 5.4, 0.7 Hz, 1H), 7.63 (d, *J* = 2.5 Hz, 1H), 6.89–6.79 (m, 2H), 5.83 (s, 2H), 4.04

(s, 3H), 2.56 (s, 3H). MS (ESI⁺) *m/z*: 256 [M + H]⁺. HRMS (ESI⁺/APCI): calcd for [C₁₃H₁₃N₅O + H]⁺, 256.1123; found, 256.1196.

The following compounds **20–28** were prepared in an analogous manner to compound **19**.

4-[4-Methoxy-2-methyl-7H-pyrrolo[2,3-d]pyrimidin-5-yl]-2-methylpyridine (20). It was isolated as a colorless solid, 15 mg (yield 45%). ¹H NMR (400 MHz, DMSO-*d*₆): δ 12.29 (s, 1H), 8.39 (dd, *J* = 5.3, 0.7 Hz, 1H), 7.81 (s, 1H), 7.64–7.59 (m, 1H), 7.54 (dd, *J* = 5.4, 1.8 Hz, 1H), 4.04 (s, 3H), 2.57 (s, 3H), 2.50 (s, 2H). MS (ESI⁺) *m/z*: 255 [M + H]⁺. HRMS (ESI⁺/APCI): calcd for [C₁₄H₁₄N₄O + H]⁺, 255.1168; found, 255.1238.

3-[4-Methoxy-2-methyl-7H-pyrrolo[2,3-d]pyrimidin-5-yl]-benzamide (21). It was isolated as a colorless solid, 16 mg (yield 26%). ¹H NMR (400 MHz, DMSO): δ 12.10 (s, 1H), 8.19 (t, *J* = 1.8 Hz, 1H), 7.99 (s, 1H), 7.83 (dd, *J* = 7.8, 1.4 Hz, 1H), 7.74 (dd, *J* = 7.8, 1.4 Hz, 1H), 7.58 (s, 1H), 7.46 (t, *J* = 7.7 Hz, 1H), 7.38 (s, 1H), 3.99 (s, 3H), 2.57 (s, 3H). MS (ESI⁺) *m/z*: 283 [M + H]⁺. HRMS (ESI⁺/APCI): calcd for [C₁₅H₁₄N₄O₂ + H]⁺, 283.1117; found, 283.1193.

2-Fluoro-4-[4-methoxy-2-methyl-7H-pyrrolo[2,3-d]pyrimidin-5-yl]pyridine (22). It was isolated as a colorless solid, 20 mg (yield 40%). ¹H NMR (400 MHz, DMSO-*d*₆): δ 12.52 (s, 1H), 8.26 (d, *J* = 5.3 Hz, 1H), 8.08 (s, 1H), 7.83 (dd, *J* = 5.4, 2.2, 1.4 Hz, 1H), 7.64–7.58 (m, 1H), 4.13 (s, 3H), 2.64 (s, 3H). MS (ESI⁺) *m/z*: 259 [M + H]⁺. HRMS (ESI⁺/APCI): calcd for [C₁₃H₁₁N₄OF + H]⁺, 259.0917; found, 259.0996.

5-(4-fluorophenyl)-4-methoxy-2-methyl-7H-pyrrolo[2,3-d]pyrimidine (23). It was isolated as a colorless solid, 40 mg (yield 55%). ¹H NMR (400 MHz, DMSO-*d*₆): δ 12.05 (s, 1H), 7.74–7.64 (m, 2H), 7.49 (s, 1H), 7.27–7.16 (m, 2H), 3.99 (s, 3H), 2.56 (s, 3H). MS (ESI⁺) *m/z*: 258 [M + H]⁺. HRMS (ESI⁺/APCI): calcd for [C₁₄H₁₂N₃OF + H]⁺, 258.0964; found, 258.1043.

4-[2-Methyl-4-[(thiophen-3-yl)methoxy]-7H-pyrrolo[2,3-d]pyrimidin-5-yl]pyridine-2-amine (24). It was isolated as a colorless solid, 15 mg (yield 37%). ¹H NMR (400 MHz, DMSO-*d*₆): δ 12.26 (s, 1H), 7.88 (dd, *J* = 5.3, 0.7 Hz, 1H), 7.69 (s, 2H), 7.74–7.60 (m, 2H), 7.37 (dd, *J* = 4.9, 1.3 Hz, 1H), 6.95–6.85 (m, 2H), 5.76 (s, 2H), 5.63 (s, 2H), 2.67 (s, 3H). MS (ESI⁺) *m/z*: 338 [M + H]⁺. HRMS (ESI⁺/APCI): calcd for [C₁₇H₁₅N₅OS + H]⁺, 338.0995; found, 338.1068.

4-[2-Methyl-4-[(5-methyl-1,2-oxazol-3-yl)methoxy]-7H-pyrrolo[2,3-d]pyrimidin-5-yl]pyridine (25). It was isolated as a colorless solid, 8 mg (yield 38%). ¹H NMR (400 MHz, DMSO-*d*₆): δ 12.41 (s, 1H), 8.50–8.44 (m, 2H), 7.89 (s, 1H), 7.79–7.72 (m, 2H), 6.38 (d, *J* = 1.1 Hz, 1H), 5.59 (s, 2H), 2.59 (s, 3H), 2.45 (s, 3H). MS (ESI⁺) *m/z*: 322 [M + H]⁺. HRMS (ESI⁺/APCI): calcd for [C₁₇H₁₅N₅O₂ + H]⁺, 322.1226; found, 322.1299.

2-Methyl-4-[(1,3-thiazol-4-yl)methoxy]-7H-pyrrolo[2,3-d]pyrimidin-5-yl]pyridine-2-amine (26). It was isolated as a colorless solid, 3 mg (yield 6%). ¹H NMR (400 MHz, DMSO-*d*₆): δ 12.28 (s, 1H), 9.24 (d, *J* = 2.0 Hz, 1H), 7.88–7.80 (m, 2H), 7.72 (s, 1H), 6.97–6.90 (m, 1H), 6.92 (s, 2H), 5.79–5.71 (m, 4H), 2.66 (s, 3H). MS (ESI⁺) *m/z*: 339 [M + H]⁺. HRMS (ESI⁺/APCI): calcd for [C₁₆H₁₄N₆OS + H]⁺, 339.0948; found, 339.1019.

4-[2-Methyl-4-[(1,3-thiazol-5-yl)methoxy]-7H-pyrrolo[2,3-d]pyrimidin-5-yl]pyridine-2-amine (27). It was isolated as a colorless solid, 10 mg (yield 40%). ¹H NMR (399 MHz, DMSO): δ 12.24 (s, 1H), 9.10 (d, *J* = 0.8 Hz, 1H), 8.09 (d, *J* = 0.9 Hz, 1H), 7.85–7.79 (d, 1H), 7.64 (s, 1H), 6.81 (dd, 2H), 5.82 (s, 2H), 5.75 (s, 2H), 2.63 (s, 3H). MS (ESI⁺) *m/z*: 339 [M + H]⁺. HRMS (ESI⁺/APCI): calcd for [C₁₆H₁₄N₆OS + H]⁺, 339.0948; found, 339.1025.

4-[4-(Benzyloxy)-2-methyl-7H-pyrrolo[2,3-d]pyrimidin-5-yl]pyridine (28). It was isolated as a colorless solid, 22 mg (yield 75%). ¹H NMR (400 MHz, DMSO-*d*₆): δ 12.35 (s, 1H), 8.41–8.35 (m, 2H), 7.86 (s, 1H), 7.77–7.70 (m, 2H), 7.57–7.49 (m, 2H), 7.47–7.32 (m, 3H), 5.57 (s, 2H), 2.60 (s, 3H). MS (ESI⁺) *m/z*: 317 [M + H]⁺. HRMS (ESI⁺/APCI): calcd for [C₁₉H₁₆N₄O + H]⁺, 317.1324; found, 317.1391.

The following compounds were prepared in parallel in an analogous manner to **34**. To a solution of the SEM-protected precursor in THF (5 mL) was added ethylenediamine (5 equiv)

followed by TBAF (1 M in THF, 5 equiv), and the mixture was stirred at 80 °C for 3 h. The individual reaction mixtures were concentrated under vacuum and evaporated onto ISOLUTE. Purification was performed by flash column chromatography followed by trituration with acetonitrile (3 × 2 mL), and the resultant solids were collected via filtration. The solids were washed lightly with diethyl ether (2 mL) and then dried under vacuum. The purified compounds were characterized by LCMS and ¹H NMR.

4-[4-(benzylamino)-2-methyl-7H-pyrrolo[2,3-d]pyrimidin-5-yl]pyridine-2-amine (29). It was isolated as a colorless solid, 51 mg (0.15 mmol) (yield 21%). ¹H NMR (400 MHz, DMSO-*d*₆): δ 11.78–11.72 (m, 1H), 7.88 (dd, *J* = 0.71, 5.18 Hz, 1H), 7.42–7.28 (m, 4H), 7.33–7.19 (m, 2H), 6.60–6.49 (m, 2H), 5.99–5.88 (m, 3H), 4.70 (d, *J* = 5.61 Hz, 2H), 2.42 (s, 3H). MS (ESI⁺) *m/z*: 331[M + H]⁺. HRMS (ESI⁺/APCI): calcd for [C₁₉H₁₈N₆+H]⁺, 331.1593; found, 331.1589.

4-(2-Methyl-4-[(thiophen-2-yl)methyl]amino)-7H-pyrrolo[2,3-d]pyrimidin-5-yl]pyridine-2-amine (30). It was isolated as a colorless solid, 31 mg (0.09 mmol) (yield 24%). ¹H NMR (400 MHz, DMSO-*d*₆): δ 11.77 (s, 1H), 7.91 (dd, *J* = 0.73, 5.24 Hz, 1H), 7.36 (dd, *J* = 1.26, 5.14 Hz, 1H), 7.25 (d, *J* = 1.65 Hz, 1H), 7.08–7.01 (m, 1H), 6.94 (dd, *J* = 3.43, 5.11 Hz, 1H), 6.58–6.46 (m, 2H), 6.07 (t, *J* = 5.86 Hz, 1H), 5.94 (s, 2H), 4.86 (d, *J* = 5.60 Hz, 2H), 2.47 (s, 3H). MS (ESI⁺) *m/z*: 337[M + H]⁺. HRMS (ESI⁺/APCI): calcd for [C₁₇H₁₆N₆S + H]⁺, 337.1149; found, 337.1222.

4-(2-Methyl-4-[(thiophen-3-yl)methyl]amino)-7H-pyrrolo[2,3-d]pyrimidin-5-yl]pyridine-2-amine (31). It was isolated as a colorless solid, 54 mg (0.16 mmol) (yield 45%). ¹H NMR (400 MHz, DMSO-*d*₆): δ 11.75 (s, 1H), 7.90 (d, *J* = 5.20 Hz, 1H), 7.49 (dd, *J* = 2.93, 4.95 Hz, 1H), 7.38 (d, *J* = 3.33 Hz, 1H), 7.24 (s, 1H), 7.15 (dd, *J* = 1.35, 4.91 Hz, 1H), 6.57 (dd, *J* = 1.55, 5.17 Hz, 1H), 6.51 (s, 1H), 5.98 (s, 2H), 5.83 (t, *J* = 5.57 Hz, 1H), 4.68 (d, *J* = 5.42 Hz, 2H), 2.45 (s, 3H). MS (ESI⁺) *m/z*: 337[M + H]⁺. HRMS (ESI⁺/APCI): calcd for [C₁₇H₁₆N₆S + H]⁺, 337.1157; found, 337.1231.

4-(4-[(Furan-3-yl)methyl]amino)-2-methyl-7H-pyrrolo[2,3-d]pyrimidin-5-yl]pyridine-2-amine (32). It was isolated as a colorless solid, 30 mg (0.09 mmol) (yield 24%). ¹H NMR (400 MHz, DMSO-*d*₆): δ 11.78–11.72 (m, 1H), 7.91 (dd, *J* = 0.70, 5.18 Hz, 1H), 7.66–7.57 (m, 2H), 7.24 (d, *J* = 2.03 Hz, 1H), 6.59–6.52 (m, 2H), 6.50 (dd, *J* = 0.77, 1.60 Hz, 1H), 5.99 (s, 2H), 5.68 (t, *J* = 5.45 Hz, 1H), 4.51 (d, *J* = 5.23 Hz, 2H), 2.46 (s, 3H). MS (ESI⁺) *m/z*: 321[M + H]⁺. HRMS (ESI⁺/APCI): calcd for [C₁₇H₁₆N₆O + H]⁺, 320.1394; found, 321.1466.

4-(2-Methyl-4-[(1,3-thiazol-4-yl)methyl]amino)-7H-pyrrolo[2,3-d]pyrimidin-5-yl]pyridine-2-amine (33). It was isolated as a colorless solid, 6 mg (0.02 mmol) (yield 3%). ¹H NMR (400 MHz, DMSO-*d*₆): δ 11.78 (s, 1H), 9.07 (d, *J* = 1.96 Hz, 1H), 7.92 (d, *J* = 5.26 Hz, 1H), 7.53 (dd, *J* = 1.02, 2.03 Hz, 1H), 7.26 (d, *J* = 2.44 Hz, 1H), 6.60 (dd, *J* = 1.53, 5.19 Hz, 1H), 6.53 (d, *J* = 1.72 Hz, 1H), 6.09 (q, *J* = 4.64, 5.62 Hz, 1H), 5.96 (s, 2H), 4.88–4.79 (m, 2H), 3.22–3.12 (m, 3H), 2.43 (s, 3H), 1.57 (dt, *J* = 7.32, 15.32 Hz, 3H), 1.32 (h, *J* = 7.35 Hz, 3H), 0.94 (t, *J* = 7.35 Hz, 4H). MS (ESI⁺) *m/z*: 338[M + H]⁺. HRMS (ESI⁺/APCI): calcd for [C₁₆H₁₅N₇S + H]⁺, 337.1114; found, 338.1189.

4-(4-[(3,5-Difluorophenyl)methyl]amino)-2-methyl-7H-pyrrolo[2,3-d]pyrimidin-5-yl]pyridine-2-amine (34). **Step 1.** 5-Bromo-*N*-[(3,5-difluorophenyl)methyl]-2-methyl-7-[[2-(trimethylsilyl)ethoxy]methyl]-7H-pyrrolo[2,3-d]pyrimidin-4-amine (46). To a solution of 43 (5 g, 13.3 mmol) in ethanol (50 mL) was added 2,6-difluorobenzylamine (Combi-Blocks SS-4198) (3.17 mL, 26.5 mmol, 2 equiv) and TEA (5.5 mL, 39.8 mmol, 5 equiv) and heated at 80 °C for 16 h. The reaction mixture was concentrated under vacuum, and the residue was retaken up in EtOAc (100 mL), washed with water and brine, and dried over anhydrous magnesium sulfate. The filtered organics were evaporated and dry-loaded onto ISOLUTE, and purification was performed by flash column chromatography (120 g silica column) to furnish the title compound as clear oil, 5.56 g (yield 87%). ¹H NMR (400 MHz, DMSO-*d*₆): δ 7.55 (s, 2H), 7.46 (tt, *J* = 8.6, 6.6 Hz, 2H), 7.23–7.11 (m, 4H), 6.80 (t, *J* = 5.9 Hz, 2H), 5.51 (s, 4H), 4.92 (d, *J* = 5.8 Hz, 4H), 3.62–3.53

(m, 4H), 2.49 (s, 6H), 1.27 (t, *J* = 7.1 Hz, 1H), 1.00–0.85 (m, 4H). MS (ESI⁺) *m/z*: 485[M + H]⁺.

5-Bromo-*N*-[(3,5-difluorophenyl)methyl]-2-methyl-7-[[2-(trimethylsilyl)ethoxy]methyl]-7H-pyrrolo[2,3-d]pyrimidin-4-amine (47). 46 (5.6 g, 11.5 mmol) and 2-aminopyridine-4-boronic acid pinacol ester (Combi-Blocks PN-0151) (4.3 g, 13.8 mmol, 1.2 equiv) were dissolved in a mixture of THF and water (4:1, 200 mL) under N₂. The mixture was treated with potassium carbonate (4.9 g, 36 mmol, 3 equiv) and Pd-118 (375 mg, 5 mol %), and the mixture was degassed with a stream of N₂ for 5 min. The whole mixture was heated up to 60 °C for 16 h, and the reaction was monitored by LCMS. The reaction mixture was cooled to rt, filtered through a plug of celite, and diluted with ethyl acetate. The organic layer was washed with brine, dried over anhydrous magnesium sulfate, concentrated under vacuum, and dry-loaded by evaporation onto ISOLUTE. Purification was performed by flash column chromatography (120 g silica). Trituration with iso-hexane gave a suspended solid which was collected by filtration and dried under vacuum to furnish the title compound as a colorless solid, 4.33 g (yield: 76%). MS (ESI⁺) *m/z*: 497[M + H]⁺.

4-(4-[(3,5-Difluorophenyl)methyl]amino)-2-methyl-7H-pyrrolo[2,3-d]pyrimidin-5-yl]pyridine-2-amine (34).

To a solution of 47 (1 equiv) in THF (100 mL) was added ethylenediamine (6 equiv) followed by TBAF (1 M solution in THF, 6 equiv), and the reaction mixture was heated to 80 °C for a total of 14 h. The reaction mixture was cooled, diluted with ethyl acetate (100 mL), washed with water (2 × 100 mL) and brine, dried over anhydrous magnesium sulfate, and concentrated under vacuum. The residue was triturated to a solid using ethyl acetate and acetonitrile, followed by diethyl ether, and the solid was collected by filtration. The solid product was dried under vacuum to give the title compound as a colorless solid, 1.89 g (yield 59%). ¹H NMR (400 MHz, DMSO-*d*₆): δ ppm 11.75 (s, 1H), 7.90 (d, *J* = 5.18 Hz, 1H), 7.37 (m, *J* = 6.61, 8.41 Hz, 1H), 7.24 (d, *J* = 2.29 Hz, 1H), 7.09 (t, *J* = 7.94 Hz, 2H), 6.54–6.45 (m, 2H), 5.93 (s, 2H), 5.85 (t, *J* = 5.79 Hz, 1H), 4.77 (d, *J* = 5.65 Hz, 2H), 2.43 (s, 3H). MS (ESI⁺) *m/z*: 367[M + H]⁺. HRMS (ESI⁺/APCI): calcd for [C₁₉H₁₆N₆F₂+H]⁺, 367.1405; found, 367.1471.

4-(4-[(3,5-Difluorophenyl)methyl]amino)-2-methyl-7H-pyrrolo[2,3-d]pyrimidin-5-yl]pyrimidin-2-amine (35). **Step 1.** 7-(Benzenesulfonyl)-5-bromo-4-chloro-2-methyl-7H-pyrrolo[2,3-d]pyrimidine (48). To a solution of 5-bromo-4-chloro-2-methyl-7H-pyrrolo[2,3-d]pyrimidine (Combi-Blocks QV-2886) (1.86 g, 7.55 mmol) in DMF (40 mL) was added sodium hydride (60% oil dispersion) (332 mg, 8.3 mmol, 1.1 equiv) at 0 °C under nitrogen. The reaction mixture was stirred at 0 °C for 30 min before adding benzene sulfonyl chloride (1.16 mL, 9 mmol, 1.2 equiv) at 0 °C. The reaction mixture was allowed to warm to room temperature gradually, and stirring was continued under nitrogen for 16 h. The reaction mixture was poured into water (50 mL) and stirred at room temperature for 20 min to break up the precipitated solid. The resulting fine precipitate was collected by filtration and washed several times with water and air-dried on a sintered funnel to furnish the title compound as a white solid, 2.64 g (yield 91%). MS (ESI⁺) *m/z*: 387[M + H]⁺.

7-(Benzenesulfonyl)-5-bromo-*N*-[(3,5-difluorophenyl)methyl]-2-methyl-7H-pyrrolo[2,3-d]pyrimidin-4-amine (49). To a suspension of 48 (1 g, 2.59 mmol) in ethanol (20 mL) was added 2,6-difluorobenzylamine (0.62 mL, 5.17 mmol, 2 equiv) and triethylamine (1 mL, 7.8 mmol, 3 equiv), and the mixture was heated at 80 °C for 16 h. The clear reaction mixture was cooled to rt upon which a yellow precipitate was formed. Water (30 mL) was added, and the suspension was stirred for ~20 min before the precipitate was collected by filtration. The solid filter cake was washed further with water and air-dried on the filter thoroughly before washing with iso-hexane. The solid was then dried under vacuum to furnish the title compound as a colorless solid, 1.19 g (yield 93%). ¹H NMR (400 MHz, DMSO-*d*₆): δ 8.17–8.09 (m, 2H), 7.81–7.71 (m, 2H), 7.65 (dd, *J* = 8.5, 7.2 Hz, 2H), 7.35 (m, *J* = 8.4, 6.6 Hz, 1H), 7.13–6.97 (m, 3H), 4.77 (d, *J* = 5.7 Hz, 2H), 3.31 (s, 1H), 2.41 (s, 3H).

7-(Benzenesulfonyl)-N-[(3,5-difluorophenyl)methyl]-2-methyl-5-(4,4,5,5-tetramethyl-1,3,2-dioxaborolan-2-yl)-7H-pyrrolo[2,3-d]pyrimidin-4-amine (**50**). To a microwave vial was added **49** (1 g 2 mmol), bis(pinacolato)diboron (617 mg, 2.43 mmol, 1.2 equiv), and KOAc (600 mg 6 mmol 3 equiv), and the mixture was dissolved in THF (15 mL) and sparged with a stream of N₂ for 10 min. PdCl₂(PPh₃)₂ (70 mg, 5 mol %) was then added, and the mixture was heated to 140 °C for 1 h. LCMS showed the target product and also some des-bromo byproduct. The cooled reaction mixture was diluted with ethyl acetate (50 mL) and washed with saturated brine solution, and the organics were dried over anhydrous magnesium sulfate. The filtered organics were reduced in volume under vacuum and dry-loaded onto ISOLUTE by evaporation. The product was purified via automated chromatography, eluting gradient 0–20% ethyl acetate/iso-hexane, and fractions were evaporated to furnish the title compound as a colorless solid, 0.68 g (yield 61%). MS (ESI⁺) *m/z*: 541[M + H]⁺.

4-[7-(Benzenesulfonyl)-4-[(3,5-difluorophenyl)methyl]amino]-2-methyl-7H-pyrrolo[2,3-d]pyrimidin-5-ylpyrimidin-2-amine (**51**). **50** (915 mg, 1.69 mmol), 2-amino-4-chloropyrimidine (329 mg, 2.54 mmol, 1.5 equiv), and K₂CO₃ (700 mg 5 mmol, 3 equiv) were combined in a microwave vial and dissolved in a mixture of THF (16 mL)/water (4 mL). The mixture was sparged with a stream of N₂ for 10 min before treatment with Pd118 (55 mg 5 mol %), and the reaction mixture was heated to 90 °C for 2 h in a CEM microwave. The reaction mixture was diluted with dichloromethane (200 mL) and washed with water (200 mL). The organics were separated, dried over MgSO₄, and concentrated under vacuum. The residue was triturated with acetonitrile to furnish a light beige solid, 551 mg (yield 64%). ¹H NMR (400 MHz, DMSO-*d*₆): δ 8.44 (s, 1H), 8.29 (d, *J* = 5.3 Hz, 1H), 8.20–8.13 (m, 2H), 7.80–7.71 (m, 1H), 7.65 (dd, *J* = 8.5, 7.1 Hz, 2H), 7.37 (d, *J* = 5.4 Hz, 1H), 7.30 (m, *J* = 14.8, 8.4, 6.5 Hz, 1H), 7.01 (t, *J* = 7.9 Hz, 2H), 6.70 (s, 2H), 4.90 (d, *J* = 5.9 Hz, 2H), 3.31 (s, 1H), 2.38 (s, 3H). MS (ESI⁺) *m/z*: 508[M + H]⁺.

4-[(3,5-Difluorophenyl)methyl]amino-2-methyl-7H-pyrrolo[2,3-d]pyrimidin-5-ylpyrimidin-2-amine (**35**). To a suspension of **51** (550 mg, 1.08 mmol) in methanol (10 mL) was added K₂CO₃ (~1.4 g, 10 mmol, excess) and stirred at room temperature for 16 h. The suspension was filtered, and the solids were washed with further methanol. The solid residue was then washed several times with water to remove the remaining inorganics, and the remaining solid was air-dried on the filter thoroughly before lightly washing with hexane. The resultant solid was dried under a vacuum oven at 60 °C to give the title compound as a colorless solid, 159 mg, (yield 40%). ¹H NMR (400 MHz, DMSO-*d*₆): δ ppm 11.96 (s, 1H), 8.14 (d, *J* = 5.41 Hz, 1H), 8.04 (s, 1H), 7.33 (m, *J* = 7.25 Hz, 1H), 7.12 (d, *J* = 5.44 Hz, 1H), 7.05 (t, *J* = 7.80 Hz, 2H), 6.34 (s, 2H), 4.91 (d, *J* = 5.84 Hz, 2H), 3.39 (s, 1H), 2.36 (s, 3H), 1.24 (s, 1H). MS (ESI⁺) *m/z*: 368[M + H]⁺. HRMS (ESI⁺/APCI): calcd for [C₁₈H₁₅N₇F₂+H]⁺, 368.1357; found, 368.1413.

4-[4-(2H-1,3-benzodioxol-5-yl)-2-methyl-7H-pyrrolo[2,3-d]pyrimidin-5-yl]pyridine-2-amine (**37**). **Step 1**. 4-(2H-1,3-benzodioxol-5-yl)-2-methyl-7H-pyrrolo[2,3-d]pyrimidine (**52**). A mixture of 4-chloro-2-methyl-7H-pyrrolo[2,3-d]pyrimidine (Combi-Blocks ST-3008) (502 mg, 3 mmol), 3,4-(methylenedioxy)-phenyl boronic acid (522 mg, 3.15 mmol), and (2 g, 6 mmol, 2 equiv) of cesium carbonate was treated with a spatula tip of the palladium(dppf)Cl₂ catalyst, and the whole mixture was suspended in 10 mL of tetrahydrofuran and 1 mL of water in a microwave vessel. The whole mixture was degassed by a stream of nitrogen for 10 min. The sealed vessel and contents were heated to 130 °C for 45 min, and the reaction mixture was allowed to cool. LCMS showed a single product peak. The reaction mixture was diluted with 150 mL of water, the solid was collected by filtration, and the filter cake was dried under vacuum in air on a sinter funnel to furnish the title compound, 750 mg, as a colorless solid (yield quant). MS (ESI⁺) *m/z*: 254[M + H]⁺.

tert-Butyl 4-(2H-1,3-benzodioxol-5-yl)-5-bromo-2-methyl-7H-pyrrolo[2,3-d]pyrimidine-7-carboxylate (**53**). **52** (750 mg 2.96 mmol) was dissolved in anhydrous DMF under N₂ and cooled to 0 °C. *N*-bromosuccinamide (600 mg 3.35 mmol, 1.1 equiv) was then

added portionwise over ~15 min. The reaction mixture was allowed to stir, slowly warming to room temperature over 2 h. The mixture was then treated with boc-anhydride (800 mg 3.67 mmol 1.2 equiv), DMAP (5 mg 0.01 equiv), and triethylamine, and stirring at room temperature was continued for a further 16 h. Water was added, and the mixture was extracted with ethyl acetate twice. The combined organics were washed with saturated brine solution (aq) and dried over anhydrous magnesium sulfate. The filtered organics were concentrated under vacuum and purified via automated column chromatography on 24 g SiO₂ cartridge eluting hexane—55% ethyl acetate/hexane mixture. Selected fractions were evaporated, and the resultant solid was dried under vacuum to furnish the title compound as off-white powder, 697 mg (yield 54%). ¹H NMR (400 MHz, DMSO-*d*₆): δ 8.00 (s, 1H), 7.23–7.13 (m, 2H), 7.07 (d, *J* = 8.0 Hz, 1H), 6.14 (s, 2H), 2.72 (s, 3H), 1.63 (s, 9H). MS (ESI⁺) *m/z*: 431.8[M + H]⁺.

4-[4-(2H-1,3-benzodioxol-5-yl)-2-methyl-7H-pyrrolo[2,3-d]pyrimidin-5-yl]pyridine-2-amine (**37**). **53** (432 mg 1 mmol), K₂CO₃ (415 mg 3 mmol 3 equiv), and boc-2-aminopyridine-4-boronic acid pinacol ester (Combi-Blocks PN-6264) (352 mg 1.1 mmol 1.1 equiv) were combined and dissolved in a mixture of THF (15 mL) and water (4 mL). The mixture was sparged with N₂ for 10 min, and the catalyst Pd118 (33 mg, 5 mol %) was then added. The whole mixture was then heated to 65 °C for 16 h. The reaction mixture was diluted with dichloromethane and washed with water, followed by saturated brine solution. The organics were then dried over anhydrous magnesium sulfate and concentrated under vacuum. The residue was purified via automated column chromatography on the 24 g SiO₂ cartridge eluting neat hexane to 10% ethyl acetate/hexane. The purified intermediate boc-protected compound was dissolved in methanol (2 mL) and treated with 1.25 M HCl in MeOH (4 mL, 5 mmol, 5 equiv), and the solution was heated in a CEM microwave at 90 °C for 1 h. Solvents were then removed *in vacuo*, residues were taken up in 2:1 dichloromethane/isopropanol and washed with saturated sodium bicarbonate solution (aq), and the organics were dried over anhydrous magnesium sulfate and evaporated to dryness. The residue solid was triturated in diethyl ether and collected by filtration. The solid filter cake was dried under vacuum to furnish the title compound as a colorless solid, 95 mg (yield 27%). ¹H NMR (400 MHz, DMSO-*d*₆): δ ppm 12.28 (s, 1H), 7.68 (s, 1H), 7.60 (dd, *J* = 0.72, 5.30 Hz, 1H), 6.98 (d, *J* = 1.66 Hz, 1H), 6.85 (dd, *J* = 1.68, 8.04 Hz, 1H), 6.74 (d, *J* = 8.02 Hz, 1H), 6.16 (dd, *J* = 0.77, 1.57 Hz, 1H), 6.02 (s, 2H), 6.05–5.98 (m, 1H), 5.65 (s, 2H), 2.69 (s, 3H). MS (ESI⁺) *m/z*: 346[M + H]⁺. HRMS (ESI⁺/APCI): calcd for [C₁₉H₁₅N₅O₂+H]⁺, 346.1226; found, 346.1127.

Protein Production. Three protein constructs of DYRK1A were used for crystal structure determination.

His-TEV-DYRK1A(127–485) was used to generate crystals of Dyk1a with ADPNP, **3**, **8**, and **10** bound. This is the same construct as that used for the published structure (2VX3³¹), removing the DYRK homology (DH) domain and the C terminus. Electron density was not observed for the initial *N*-terminal amino acids; a construct was therefore designed with slightly truncated *N* and *C* terminal sequences with a thrombin cleavage site (His-thrombin-DYRK1A-(148–479-ala-ala)) which generated crystals of Dyk1a with **1** and **6** bound. A further construct was designed (His-thrombin-DYRK1A(148–485)) for all other crystal structures reported here.

A clone codon optimized for expression in *Escherichia coli* for His-TEV-DYRK1A(127–485) in pET21a was generated by gene synthesis (Celtek BioScience, USA). This clone was used as a template for PCR to generate an *N*-terminal truncation ligated to pET15b, His-thrombin-DYRK1A(148–485), and subsequent site-directed mutagenesis (Agilent) yielded a *C*-terminal truncate, His-Thrombin-DYRK1A(148–479-ala-ala). *E. coli* BL21(DE3) pLysS were transformed with the DYRK1A encoding plasmid and cultured at 37 °C in Luria–Bertani (LB) supplemented with 100 μg/mL ampicillin. Once the culture had reached an O.D.600 nm of 0.4, the incubator temperature was reduced to 22 °C. At O.D.600 nm of 0.6, expression was induced by the addition of 1 mM IPTG (final

concentration). The cells were pelleted after 16 hrs and stored at -80°C .

A similar protein purification protocol was used for all constructs. Cell pellets were resuspended in lysis buffer [50 mM *N*-(2-hydroxyethyl)piperazine-*N'*-ethanesulfonic acid (HEPES) pH 7.5, 500 mM NaCl, 5% glycerol containing ethylenediaminetetraacetic acid (EDTA)-free protease inhibitor cocktail (Roche) and DNase I (Sigma)] and lysed by mechanical homogenization. The lysate was centrifuged at 20,000 rpm for 60 mins, 4°C . The clarified lysate was applied to a 1 mL HiTrap chelating column (Cytiva) charged with Ni^{2+} pre-equilibrated with lysis buffer. After washing the column, the protein of interest was eluted using a series of step gradients of lysis buffer + 500 mM imidazole. Sodium dodecyl sulfate polyacrylamide gel electrophoresis (SDS-PAGE) analysis confirmed the fractions of interest which were pooled and concentrated using an Amicon Ultra 30 kDa MWCO concentrator (Merck Millipore). The sample was applied to a HiLoad 16/60 Superdex 75 pg size exclusion chromatography column (Cytiva) pre-equilibrated in 50 mM HEPES pH 7.5, 500 mM NaCl, and 5 mM DTT. Samples were analyzed by SDS-PAGE and concentrated using an Amicon 30 kDa MWCO concentrator (Merck Millipore) to 18 mg/mL. The purified protein was aliquoted and snap-frozen prior to being stored at -80°C .

If required, the *N*-terminal His-tag was removed by incubation overnight at 4°C , with AcTEV protease (ThermoFisher) at 1 U/3 μg purified protein after affinity chromatography. A repeated affinity purification resulted in the protein of interest in the nonabsorbed fraction before size exclusion chromatography was performed.

Fragment Screen. All protein NMR spectra were measured on a 600 MHz Bruker AVANCE III spectrometer fitted with a cryoprobe. Ligand-observed fragment screening was performed with 500 μM of each compound, 10 μM Dyrk1a (produced from His-TEV-DYRK1A(127–485) with the tag removed) in 20 mM HEPES pH 7.4, and 15 μM NaCl, in mixtures of six compounds per sample as described previously.^{35,36}

Crystallization of Dyrk1a. Crystal structures of different ligands complexed to Dyrk1a were obtained using the following protein constructs—AMPNP; compounds 3, 8, 10, and 34 with His-TEV-DYRK1A (aa127–485); compounds 1 and 6 with His-Thrombin-DYRK1A (148–479-Ala-Ala); and all others with His-Thrombin-DYRK1A (aa127–485).

For all compounds other than 34, crystals were prepared by replacement of AMPNP from Dyrk1a/AMPNP crystals. Purified Dyrk1a protein (all constructs) at ~ 15 mg/mL concentration was mixed with fourfold excess (molar ratio) of AMPNP in vapor diffusion experiments. The best crystals were obtained from a solution containing 0.1 M MES buffer at pH 6.5, 12% Peg3350, and 0.2 M MgCl_2 at 20°C . To replace the AMPNP, the crystals were soaked for ~ 24 h in a crystallization solution containing 4–10 mM ligand (final DMSO concentration of 10–20%).

Crystals of the complex of Dyrk1a with 34 were obtained from a protein solution at ~ 15 mg/mL mixed with approximately fourfold excess of 34 (final DMSO concentration of 8%) that had been incubated overnight. Crystals appeared from vapor diffusion experiments, with the best crystals obtained from conditions containing 0.1 M HEPES buffer at pH 7.5, 20% Peg4 k, and 0.2 M MgCl_2 , also at 20°C .

Crystallographic Data Collection. Crystals were cryoprotected in a solution of crystallization buffer enriched in glycerol up to 20–25% and flash frozen in liquid nitrogen. Table S1 summarizes the data collection statistics, with data obtained from ESRF (beamline id23-1) or DLS (i02, i03, and i04 beamlines). Data were processed and scaled with DENZO/Scalepack package⁴⁹ or XDS⁵⁰ software.

Structure Determination. Structures of Dyrk1a complexes were solved by molecular replacement (MolRep⁵¹) using the coordinates from PDB code 2VX3⁵¹ as a model.

The refined structure of the relevant protein construct (stripped of the compound) was used as a starting model for solving (by molecular replacement) subsequent structures of the complexes with ligands. After structure solution, several cycles of refinement were conducted

with Refmac5⁵² software from the CCP4 package,⁵³ alternating with manual rebuilding using the program COOT.⁵⁴ Compounds were modeled in the surplus peaks in the difference Fourier electron density maps. Topology files for the ligands were created by ProDrug,⁵⁵ also from within the CCP4 package. Refinement statistics for each new structure reported in this paper are in Table S2.

Protein Kinase Assays. A number of different assay formats were used to measure inhibition of different kinases by compounds described in this paper.

ADP Hunter Plus (DiscoverX) was used to measure the activity of the protein kinases DYRK1A, PAK4, Pim1, Aurora A, and DYRK2.

A TR-FRET assay was used to measure the activity of the protein kinases DYRK1A, DYRK1B, DYRK2, DYRK3, DYRK4, CDK9, and CLK1.

The K_d for binding of compounds to kinases was determined in an 11-point threefold serial dilution in the KINOMEScan assay available at DiscoveRx (now Eurofins).

A radiometric assay was used to measure the activity of the protein kinase GSK3- β .

The inhibition of TTK was measured at CEREP (now Eurofins).

ADP Hunter Plus Assay. The ADP Hunter Plus assay measures the accumulation of ADP. Protein kinase assays were performed in 96-well black plates (Corning #3686) at 30°C in a final volume of 20 μL in 50 mM HEPES, pH 7.4, 20 mM NaCl, 10 mM MgCl_2 , 1 mM EGTA, 0.01 mg/mL BGG, 0.02% Tween 20, and 2% DMSO. The order of the addition of reagents to the assay plate was 5 μL of compound/8% DMSO, 10 μL of kinase/substrate mix, and 5 μL of ATP. Final concentrations and assay conditions used are described in Table S3. Following incubation, 5 μL of Reagent A was added, followed by 10 μL of Reagent B and plate incubated for a further 20 min at 30°C . Finally, 5 μL of the stop reagent was added, and the plate was read on a Molecular Devices flexstation plate reader using Ex/Em 530/590 nm in conjunction with a 585 nm cutoff dichroic mirror.

TR-FRET Assay. The TR-FRET assay was performed on a TECAN Evo robotic platform. The compound at 5% DMSO was added to reaction buffer (50 mM HEPES pH 7.4, 1 mM EGTA, 10 mM MgCl_2 ; 2 mM DTT & 0.01% Tween20) containing 20 ng/ μL DYRK1A Kinase (Carna Biosciences #04–130), 100 μM Ulight-MBP substrate (PerkinElmer #TRF109L), and 10 μM ATP cosubstrate (Sigma-Aldrich #A2383) and incubated for 40 min at room temperature. The kinase reaction was stopped by adding 10 mM EDTA (Sigma-Aldrich #E7889) and 1 nM anti-phospho-MBP (PerkinElmer #TRF0201L) and incubated for 1 h minimum at room temperature. Plates were read on a multimode reader (PerkinElmer Envision 2400) with an excitation wavelength of 337 nm and emission wavelengths of 620 nm for the donor and 665 nm for the acceptor. A similar format was used for other TR-FRET kinase inhibition assays.

Radiometric Assay. The radiometric assay for glycogen synthase 3 β (GSK3 β) inhibition was performed in 96-well plates (Greiner; VWR #651201) at 30°C for 40 min in a final volume of 50 μL where reagents were added in the following order: 1 μL of compound/100% DMSO, 39 μL of kinase/substrate mix, and 10 μL of ATP/³³P ATP mix. Final concentrations used were 39 nM GSK3 β (Merck #14–306), 16.5 μM GSK3 β tide substrate (YRRAAVPPSPSLSRHSSPHQ-(pS)EDEEE), 10 μM ATP, 0.5 μCi ³³P ATP, 50 mM HEPES, pH 7.5, 15 mM $\text{Mg}(\text{C}_2\text{H}_3\text{O}_2)_2$, 0.01 mg/mL bovine serum albumin (BSA), and 2% DMSO. Following incubation, the assay was stopped by the addition of 50 μL of 50 mM phosphoric acid solution and 90 μL of assay reaction transferred to a prewetted filter plate, washed three times with 100 μL of 50 mM phosphoric acid solution, dried, and counted in the presence of 50 μL of scintillation fluid on a Trilux plate reader.

DYRK1A (pS520) Cell Assay. U2OS cells were transiently transfected with a plasmid expressing full length wild-type DYRK1A (pcDNA3.1). After 5 h, compounds were added, and cells were incubated for a further 5 h. Cells were lysed, and equal amounts of protein were separated by SDS-PAGE and transferred to the poly(vinylidene difluoride) membrane. Membranes were probed for pS520 DYRK1A (custom rabbit-polyclonal antibody immunized with

the synthetic peptide SNSGRARpSDPTHQHR, Eurogentec; 1:500 in 5% BSA-TBST) and detected with anti-rabbit IgG-HRP (7074, CST; 1:3000) and then quantified on an electrochemical luminescence camera (BioRad). Membranes were subsequently stripped and reprobed with a total anti-DYRK1A antibody (H0000-1859, Abnova; 1:1000 in 5% BSA-TBST) and quantified as mentioned above.

Caco2—Papp Assay. The Caco-2 cell line was cultured in adapted media and used between 21 and 30 days post seeding. The compound was incubated at 20 μ M in the apical chamber in HBSS buffer containing 0.1% BSA. Samples (duplicate) were collected at 30 and 90 min in the basolateral chamber and analyzed by HPLC-LC/MS/MS. The apparent permeability was calculated as follows: $P_{app} (\text{cm/s}) = K \cdot V_r / A \cdot 60$, where V_r is the volume of the receiver chamber (mL), A is the surface area of the membrane (cm^2), and K is the slope of the cumulated absorbed fraction as a function of time (min^{-1}).

Metabolic Stability (Mouse/Rat/Human). Pooled liver microsomes from mouse (CD-1), rat (Sprague–Dawley), and human liver microsomes (mixed gender) are used with a final microsomal protein concentration of 0.3 mg/mL. The compound (0.1 μ M) was tested in duplicate. After preincubation with pooled liver microsomes (10 min, 37 $^{\circ}$ C), the reaction is initiated by adding a reduced nicotinamide adenine dinucleotide phosphate-generating system and incubated in a 37 $^{\circ}$ C shaking water bath. Samples were collected at different time points (0, 7, 17, 30, and 45 min), and the reaction was stopped by a mixture of 20 nM antipyrine and 0.1% formic acid in acetonitrile/methanol/water (35/35/30, v/v/v). Samples were analyzed by HPLC-MS/MS.

The hepatic blood clearance was extrapolated using the following equation

$$Cl_H (\text{mL/min}) = \frac{Cl_{int} \times LW \times sc \times Q_h \times f_u}{(Cl_{int} \times LW \times sc \times f_u) + Q_h}$$

where LW is the liver weight (g), sc is the scaling factor (g protein/g liver), Q_h is the hepatic blood flow (mL/min), and f_u is the blood unbound fraction (1 by default), and the intrinsic clearance (Cl_{int}) is as follows

$$Cl_{int} (\mu\text{L/min /mg protein}) = \frac{0.693}{t_{1/2} \times \text{protein concentration}}$$

Plasma protein Binding (Mouse/Human) Assay. Each pool of mouse and human plasma was spiked with the compound to obtain a final concentration of 5 μ M. Dialysis was performed (in triplicate) using 300 μ L of each plasma spiked (donor chamber) and 500 μ L of phosphate buffer pH 7.4 (receiver chamber). All replicates were incubated for 3 h at 37 $^{\circ}$ C using rapid equilibrium dialysis (device-Pierce) under orbital stirring. All plasma and buffer samples (40 μ L) were analyzed with the HPLC-LC-MS/MS method.

The extent of plasma protein binding in each sample was calculated as follows

$$f_u (\%) = C_u / C_{pl} \times 100$$

Where f_u is the unbound fraction expressed as a percentage, C_{pl} is the concentration of the compound in the plasma at the end of dialysis, and C_u is the concentration of the unbound compound in the buffer. The unbound fraction (f_u %) was determined as the mean of the unbound fraction calculated from the triplicate.

hERG Assay. The effect of compounds on hERG activity was studied at room temperature (22 ± 2 $^{\circ}$ C) on hERG currents in HEK-293 cells stably expressing the hERG potassium channel. Cells were maintained at a potential of -80 mV, and hERG currents were activated by cell depolarization ($+30$ mV, 1 s) followed by cell repolarization (40 mV, 1 s). Cells were incubated with DMSO 0.1% in extracellular solution for 10 min (baseline) followed by three increasing consecutive concentrations of the compound (1, 3, and 10 μ M/L, $n = 4$) until the steady state was reached. The hERG tail current amplitude was determined by the difference between the tail current amplitude upon repolarization to -40 mV and the base

current amplitude at -80 mV. The percentage of inhibition was determined as compared to the baseline.

In Vivo Efficacy Studies. Female nude mice (CrI/NU(NCr)-*Foxn1nu*) were purchased from Charles River Laboratories. Xenograft studies were undertaken by Charles River Laboratories Discovery Services, North Carolina, and accredited by the Association for Assessment and Accreditation of Laboratory Animal Care International. The U87MG tumor line was maintained by serial SC transplantation in female athymic nude mice. Tumor fragments, approximately 1 mm^3 each, were implanted SC into the right flank of each animal and allowed to grow toward a target size of 100–150 mm^3 . On day 1 of the study, tumors were randomized into treatment groups before compound administration. For tumor PK studies, the tumors were allowed to reach a target volume of 300 mm^3 prior to randomization.

Compound **34** was formulated in 60 mM HCl and 20% hydroxypropyl- β -cyclodextrin and administered by oral gavage once daily for 21 days. The tumor size was measured with electronic calipers, and the tumor volume was calculated according to the formula $((\text{width} \times \text{width}) \times \text{length})/2$. Body weight was measured daily for the first 5 days and then twice weekly thereafter. The study endpoint was defined as a tumor volume of 2000 mm^3 or D28, whichever came first. Each animal was euthanized when its tumor reached the endpoint, and the last day of the study was D28.

The time to endpoint (TTE) for each mouse was calculated from the following equation: $TTE = \log_{10} (\text{endpoint volume}) - b/m$ where b is the intercept and m is the slope of the line obtained by linear regression of a log-transformed tumor growth data set. The data set is composed of the first observation that exceeded the study endpoint volume and the three consecutive observations that immediately preceded the attainment of the endpoint volume. Animals that did not reach endpoint were euthanized at the end of the study and assigned a TTE value equal to the last day of the study (D28). Animals determined to have died from treatment-related (TR) causes were assigned a TTE value equal to the day of death. If the animal died from nontreatment-related causes, it was excluded from the TTE calculations.

The treatment outcome is evaluated by TGD, which is defined as the increase in the median TTE in a treatment group compared to the control group: $TGD = T - C$ expressed in days or as a percentage of the median TTE of the control group: $\% TGD = (T - C)/C \times 100$ where T = median TTE for a treatment group and C = median TTE for the control group.

■ ASSOCIATED CONTENT

Supporting Information

The Supporting Information is available free of charge at <https://pubs.acs.org/doi/10.1021/acs.jmedchem.1c00024>.

Supporting figures, tables and data: Compound **34** target engagement with DYRK1A demonstrated in nano-BRET assay; comparison of the conformation of equivalent leucine residues in the kinase hinge of CLK1 and Dyrk1a structures; in vivo PK characterisation of compound **34** in mice; compound **34** exhibits activity against U87MG glioblastoma cells in vitro; comparison of binding pose of **34** with recently published inhibitors of DYRK1A; crystallographic data collection; refinement statistics; final concentrations of reagents in the kinase inhibition assays; kinase profiling of **34**; brain penetrance of **34**; in vivo PK; complete list of kinome screen data; LC chromatograms, and ^1H NMR spectra of key compounds (PDF)

Molecular formula strings (CSV)

■ AUTHOR INFORMATION

Corresponding Author

Roderick E. Hubbard – Vernalis (R&D) Ltd., Cambridge CB21 6GB, U.K.; orcid.org/0000-0002-8233-7461; Email: r.hubbard@vernalis.com

Authors

David Lee Walmsley – Vernalis (R&D) Ltd., Cambridge CB21 6GB, U.K.

James B. Murray – Vernalis (R&D) Ltd., Cambridge CB21 6GB, U.K.; orcid.org/0000-0003-1007-8218

Pawel Dokurno – Vernalis (R&D) Ltd., Cambridge CB21 6GB, U.K.; orcid.org/0000-0002-7332-8889

Andrew J. Massey – Vernalis (R&D) Ltd., Cambridge CB21 6GB, U.K.; orcid.org/0000-0002-0276-2573

Karen Benwell – Vernalis (R&D) Ltd., Cambridge CB21 6GB, U.K.

Andrea Fiumana – Vernalis (R&D) Ltd., Cambridge CB21 6GB, U.K.

Nicolas Foloppe – Vernalis (R&D) Ltd., Cambridge CB21 6GB, U.K.

Stuart Ray – Vernalis (R&D) Ltd., Cambridge CB21 6GB, U.K.

Julia Smith – Vernalis (R&D) Ltd., Cambridge CB21 6GB, U.K.

Allan E. Surgenor – Vernalis (R&D) Ltd., Cambridge CB21 6GB, U.K.; orcid.org/0000-0002-9869-1430

Thomas Edmonds – Institut de Recherches Servier, Croissy-sur-Seine 78290, France

Didier Demarles – Technologie Servier, Orleans 45000, France

Mike Burbridge – Institut de Recherches Servier, Croissy-sur-Seine 78290, France

Francisco Cruzalegui – Institut de Recherches Servier, Croissy-sur-Seine 78290, France; Present Address: Francisco Cruzalegui:Evotec (France) SAS 195 Route d'Espagne 31036 Toulouse, France E-mail: cruzalegui.francisco@orange.fr

Andras Kotschy – Servier Research Institute of Medicinal Chemistry, Budapest H-1031, Hungary; orcid.org/0000-0002-7675-3864

Complete contact information is available at:

<https://pubs.acs.org/10.1021/acs.jmedchem.1c00024>

Author Contributions

The manuscript was written through contributions of all authors. All authors have given approval to the final version of the manuscript.

Notes

The authors declare no competing financial interest.

The authors thank co-workers at the Analytical Division of the Servier Research Institute of Medicinal Chemistry for providing the detailed chemical analysis of the compounds and from Vernalis, and we thank Hayley Angove for assistance with the assay protocols.

The X-ray structures of compounds complexed with Dyrk1a reported in this paper have been deposited in the PDB with the following codes. ADPNP: 7A4O, 1: 7A4R, 2: 7A4S, 3: 7A4W; 4: 7A4Z, 5: 7A51, 6: 7A52, 7: 7A53, 8: 7A55, 10: 7A5B, 16: 7A5D, 24: 7A5L, and 34: 7A5N. The authors will release the atomic coordinates and experimental data upon article publication.

■ ABBREVIATIONS

DYRK, dual-specificity tyrosine-regulated kinase; CMGC, cyclin-dependent, mitogen-activated, glycogen synthase, and CDC-like; EGFR, epidermal growth factor; GLI, glioma-associated oncogene; Mcl-1, myeloid cell leukemia 1; Bcl-2, B-cell lymphoma 2; EGCG, epigallocatechin gallate; PDB, protein databank; PK, pharmacokinetic; PD, pharmacodynamic; PAK4, p21-associated kinase 4; ADP, adenosine diphosphate; TR-FRET, time-resolved fluorescence energy transfer; GSK3 β , glycogen synthase 3 β ; ADPNP, 5'-adenylyl- β , γ -imidodiphosphate; NMR, nuclear magnetic resonance; HAC, heavy atom count; ATP, adenosine triphosphate; LE, ligand efficiency; CDK9, cyclin-dependent kinase 9; CLK, CDC-like kinase; hERG, human ether-a-go-go-related gene; HIPK2, homeodomain interacting protein kinase 2; SCID, severe combined immunodeficiency; po, per os; SAR, structure–activity relationship

■ REFERENCES

- (1) Alvarez, M.; Altafaj, X.; Aranda, S.; de la Luna, S. Dyrk1a autophosphorylation on serine residue 520 modulates its kinase activity via 14-3-3 binding. *Mol. Biol. Cell* **2007**, *18*, 1167–1178.
- (2) Mercer, S. E.; Ewton, D. Z.; Shah, S.; Naqvi, A.; Friedman, E. Mirk/dyrk1b mediates cell survival in rhabdomyosarcomas. *Cancer Res.* **2006**, *66*, 5143–5150.
- (3) Yang, C.; Ji, D.; Weinstein, E. J.; Choy, E.; Hornicek, F. J.; Wood, K. B.; Liu, X.; Mankin, H.; Duan, Z. The kinase mirk is a potential therapeutic target in osteosarcoma. *Carcinogenesis* **2010**, *31*, 552–558.
- (4) Gao, J.; Zheng, Z.; Rawal, B.; Schell, M. J.; Bepler, G.; Haura, E. B. Mirk/dyrk1b, a novel therapeutic target, mediates cell survival in non-small cell lung cancer cells. *Canc. Biol. Ther.* **2009**, *8*, 1671–1679.
- (5) Deng, X.; Ewton, D. Z.; Li, S.; Naqvi, A.; Mercer, S. E.; Landas, S.; Friedman, E. The kinase mirk/dyrk1b mediates cell survival in pancreatic ductal adenocarcinoma. *Cancer Res.* **2006**, *66*, 4149–4158.
- (6) Hu, J.; Deng, H.; Friedman, E. A. Ovarian cancer cells, not normal cells, are damaged by mirk/dyrk1b kinase inhibition. *Int. J. Cancer* **2013**, *132*, 2258–2269.
- (7) Litovchick, L.; Florens, L. A.; Swanson, S. K.; Washburn, M. P.; DeCaprio, J. A. Dyrk1a protein kinase promotes quiescence and senescence through dream complex assembly. *Genes Dev.* **2011**, *25*, 801–813.
- (8) Jin, K.; Ewton, D. Z.; Park, S.; Hu, J.; Friedman, E. Mirk regulates the exit of colon cancer cells from quiescence. *J. Biol. Chem.* **2009**, *284*, 22916–22925.
- (9) Boichuk, S.; Parry, J. A.; Makielski, K. R.; Litovchick, L.; Baron, J. L.; Zewe, J. P.; Wozniak, A.; Mehalek, K. R.; Korzeniewski, N.; Seneviratne, D. S.; Schöffski, P.; Debiec-Rychter, M.; DeCaprio, J. A.; Duensing, A. The dream complex mediates gist cell quiescence and is a novel therapeutic target to enhance imatinib-induced apoptosis. *Cancer Res.* **2013**, *73*, 5120–5129.
- (10) Becker, W. A wake-up call to quiescent cancer cells - potential use of DYRK1B inhibitors in cancer therapy. *FEBS J.* **2018**, *285*, 1203–1211.
- (11) Zou, Y.; Ewton, D. Z.; Deng, X.; Mercer, S. E.; Friedman, E. Mirk/dyrk1b kinase destabilizes cyclin d1 by phosphorylation at threonine 288. *J. Biol. Chem.* **2004**, *279*, 27790–27798.
- (12) Ashford, A. L.; Oxley, D.; Kettle, J.; Hudson, K.; Guichard, S.; Cook, S. J.; Lochhead, P. A. A novel DYRK1B inhibitor AZ191 demonstrates that DYRK1B acts independently of GSK3 β to phosphorylate cyclin D1 at Thr286, not Thr288. *Biochem. J.* **2014**, *457*, 43–56.
- (13) Deng, X.; Mercer, S. E.; Shah, S.; Ewton, D. Z.; Friedman, E. The Cyclin-dependent Kinase Inhibitor p27Kip1 Is Stabilized in G0 by Mirk/dyrk1B Kinase. *J. Biol. Chem.* **2004**, *279*, 22498–22504.
- (14) Janumyan, Y.; Cui, Q.; Yan, L.; Sansam, C. G.; Valentin, M.; Yang, E. G0 function of bcl2 and bcl-xl requires bax, bak, and p27

phosphorylation by mirk, revealing a novel role of bax and bak in quiescence regulation. *J. Biol. Chem.* **2008**, *283*, 34108–34120.

(15) Pozo, N.; Zahonero, C.; Fernandez, P.; Liñares, J. M.; Ayuso, A.; Hagiwara, M.; Pérez, A.; Ricoy, J. R.; Hernández-Lain, A.; Sepúlveda, J. M.; Sánchez-Gómez, P. Inhibition of dyrk1a destabilizes egfr and reduces egfr-dependent glioblastoma growth. *J. Clin. Invest.* **2013**, *123*, 2475–2487.

(16) Mao, J.; Maye, P.; Kogerman, P.; Tejedor, F. J.; Toftgard, R.; Xie, W.; Wu, G.; Wu, D. Regulation of glil transcriptional activity in the nucleus by dyrk1. *J. Biol. Chem.* **2002**, *277*, 35156–35161.

(17) Gruber, W.; Hutzinger, M.; Elmer, D. P.; Parigger, T.; Sternberg, C.; Cegielski, L.; Zaja, M.; Leban, J.; Michel, S.; Hamm, S.; Vitt, D.; Aberger, F. Dyrk1b as therapeutic target in hedgehog/gli-dependent cancer cells with smoothened inhibitor resistance. *Oncotarget* **2016**, *7*, 7134–7148.

(18) Li, Y.; Zhou, D.; Xu, S.; Rao, M.; Zhang, Z.; Wu, L.; Zhang, C.; Lin, N. Dyrk1a suppression restrains mcl-1 expression and sensitizes nsccl cells to bcl-2 inhibitors. *Cancer Biol. Med.* **2020**, *17*, 387–400.

(19) Yoshida, S.; Yoshida, K. Multiple functions of dyrk2 in cancer and tissue development. *FEBS Lett.* **2019**, *593*, 2953–2965.

(20) Correa-Saez, A.; Jimenez-Izquierdo, R.; Garrido-Rodriguez, M.; Morrugares, R.; Munoz, E.; Calzado, M. A. Updating dual-specificity tyrosine-phosphorylation-regulated kinase 2 (dyrk2): Molecular basis, functions and role in diseases. *Cell. Mol. Life Sci.* **2020**, *77*, 4747–4763.

(21) Stringer, M.; Goodlett, C. R.; Roper, R. J. Targeting trisomic treatments: Optimizing dyrk1a inhibition to improve down syndrome deficits. *Mol. Genet. Genomic Med.* **2017**, *5*, 451–465.

(22) Goodlett, C. R.; Stringer, M.; LaCombe, J.; Patel, R.; Wallace, J. M.; Roper, R. J. Evaluation of the therapeutic potential of epigallocatechin-3-gallate (egcg) via oral gavage in young adult down syndrome mice. *Sci. Rep.* **2020**, *10*, 10426.

(23) Ryoo, S.-R.; Jeong, H. K.; Radnaabazar, C.; Yoo, J.-J.; Cho, H.-J.; Lee, H.-W.; Kim, I.-S.; Cheon, Y.-H.; Ahn, Y. S.; Chung, S.-H.; Song, W.-J. DYRK1A-mediated Hyperphosphorylation of Tau. *J. Biol. Chem.* **2007**, *282*, 34850–34857.

(24) Ferrer, I.; Barrachina, M.; Puig, B.; Martínez de Lagrán, M.; Martí, E.; Avila, J.; Dierssen, M. Constitutive dyrk1a is abnormally expressed in alzheimer disease, down syndrome, pick disease, and related transgenic models. *Neurobiol. Dis.* **2005**, *20*, 392–400.

(25) Kimura, R.; Kamino, K.; Yamamoto, M.; Nuripa, A.; Kida, T.; Kazui, H.; Hashimoto, R.; Tanaka, T.; Kudo, T.; Yamagata, H.; Tabara, Y.; Miki, T.; Akatsu, H.; Kosaka, K.; Funakoshi, E.; Nishitomi, K.; Sakaguchi, G.; Kato, A.; Hattori, H.; Uema, T.; Takeda, M. The DYRK1A gene, encoded in chromosome 21 Down syndrome critical region, bridges between β -amyloid production and tau phosphorylation in Alzheimer disease. *Hum. Mol. Genet.* **2007**, *16*, 15–23.

(26) Barallobre, M. J.; Perier, C.; Bové, J.; Laguna, A.; Delabar, J. M.; Vila, M.; Arbonés, M. L. Dyrk1a promotes dopaminergic neuron survival in the developing brain and in a mouse model of parkinson's disease. *Cell Death Dis.* **2014**, *5*, No. e1289.

(27) Kim, E. J.; Sung, J. Y.; Lee, H. J.; Rhim, H.; Hasegawa, M.; Iwatsubo, T.; Min, D. S.; Kim, J.; Paik, S. R.; Chung, K. C. Dyrk1A Phosphorylates α -Synuclein and Enhances Intracellular Inclusion Formation. *J. Biol. Chem.* **2006**, *281*, 33250–33257.

(28) Dirice, E.; Walpita, D.; Vetere, A.; Meier, B. C.; Kahraman, S.; Hu, J.; Dančík, V.; Burns, S. M.; Gilbert, T. J.; Olson, D. E.; Clemons, P. A.; Kulkarni, R. N.; Wagner, B. K. Inhibition of DYRK1A Stimulates Human β -Cell Proliferation. *Diabetes* **2016**, *65*, 1660–1671.

(29) Shen, W.; Taylor, B.; Jin, Q.; Nguyen-Tran, V.; Meeusen, S.; Zhang, Y. Q.; Kamireddy, A.; Swafford, A.; Powers, A. F.; Walker, J.; Lamb, J.; Bursalaya, B.; DiDonato, M.; Harb, G.; Qiu, M.; Filippi, C. M.; Deaton, L.; Turk, C. N.; Suarez-Pinzon, W. L.; Liu, Y.; Hao, X.; Mo, T.; Yan, S.; Li, J.; Herman, A. E.; Hering, B. J.; Wu, T.; Martin Seidel, H.; McNamara, P.; Glynn, R.; Laffitte, B. Inhibition of dyrk1a and gsk3b induces human beta-cell proliferation. *Nat. Commun.* **2015**, *6*, 8372.

(30) Rachdi, L.; Kariyawasam, D.; Aiello, V.; Herault, Y.; Janel, N.; Delabar, J.-M.; Polak, M.; Scharfmann, R. Dyrk1A induces pancreatic β cell mass expansion and improves glucose tolerance. *Cell Cycle* **2014**, *13*, 2221–2229.

(31) Soundararajan, M.; Roos, A. K.; Savitsky, P.; Filippakopoulos, P.; Kettenbach, A. N.; Olsen, J. V.; Gerber, S. A.; Eswaran, J.; Knapp, S.; Elkins, J. M. Structures of down syndrome kinases, dyrks, reveal mechanisms of kinase activation and substrate recognition. *Structure* **2013**, *21*, 986–996.

(32) Weber, C.; Sipos, M.; Paczal, A.; Balint, B.; Kun, V.; Fölppe, N.; Dokurno, P.; Massey, A. J.; Walmsley, D. L.; Hubbard, R. E.; Murray, J.; Benwell, K.; Edmonds, T.; Demarles, D.; Bruno, A.; Burbridge, M.; Cruzalegui, F.; Kotschy, A. Structure-Guided Discovery of Potent and Selective DYRK1A Inhibitors. *J. Med. Chem.* **2021**, DOI: 10.1021/acs.jmedchem.1c00023.

(33) Ha, B. H.; Davis, M. J.; Chen, C.; Lou, H. J.; Gao, J.; Zhang, R.; Krauthammer, M.; Halaban, R.; Schlessinger, J.; Turk, B. E.; Boggan, T. J. Type ii p21-activated kinases (paks) are regulated by an autoinhibitory pseudosubstrate. *Proc. Natl. Acad. Sci. U.S.A.* **2012**, *109*, 16107–16112.

(34) Baurin, N.; Aboul-El, F.; Barril, X.; Davis, B.; Drysdale, M.; Dymock, B.; Finch, H.; Fromont, C.; Richardson, C.; Simmonite, H.; Hubbard, R. E. Design and characterization of libraries of molecular fragments for use in nmr screening against protein targets. *J. Chem. Inf. Comput. Sci.* **2004**, *44*, 2157–2166.

(35) Hubbard, R. E.; Murray, J. B. Experiences in fragment-based lead discovery. *Methods Enzymol.* **2011**, *493*, 509–531.

(36) Hubbard, R.; Davis, B.; Chen, I.; Drysdale, M. The seeds approach: Integrating fragments into drug discovery. *Curr. Top. Med. Chem.* **2007**, *7*, 1568–1581.

(37) Hopkins, A. L.; Groom, C. R.; Alex, A. Ligand efficiency: A useful metric for lead selection. *Drug Discov. Today* **2004**, *9*, 430–431.

(38) Chen, I.-J.; Hubbard, R. E. Lessons for fragment library design: Analysis of output from multiple screening campaigns. *J. Comput. Aided Mol. Des.* **2009**, *23*, 603–620.

(39) Hajduk, P. J.; Huth, J. R.; Fesik, S. W. Druggability indices for protein targets derived from nmr-based screening data. *J. Med. Chem.* **2005**, *48*, 2518–2525.

(40) Halgren, T. A. Identifying and characterizing binding sites and assessing druggability. *J. Chem. Inf. Model.* **2009**, *49*, 377–389.

(41) Ogawa, Y.; Nonaka, Y.; Goto, T.; Ohnishi, E.; Hiramatsu, T.; Kii, I.; Yoshida, M.; Ikura, T.; Onogi, H.; Shibuya, H.; Hosoya, T.; Ito, N.; Hagiwara, M. Development of a novel selective inhibitor of the down syndrome-related kinase dyrk1a. *Nat. Commun.* **2010**, *1*, 86.

(42) Akue-Gedu, R.; Debiton, E.; Ferandin, Y.; Meijer, L.; Prudhomme, M.; Anizon, F.; Moreau, P. Synthesis and biological activities of aminopyrimidyl-indoles structurally related to meridianins. *Bioorg. Med. Chem.* **2009**, *17*, 4420–4424.

(43) Tazarki, H.; Zeinyeh, W.; Esvan, Y. J.; Knapp, S.; Chatterjee, D.; Schröder, M.; Joerger, A. C.; Khiari, J.; Josselin, B.; Baratte, B.; Bach, S.; Ruchaud, S.; Anizon, F.; Giraud, F.; Moreau, P. New pyrido[3,4-g]quinazoline derivatives as clk1 and dyrk1a inhibitors: Synthesis, biological evaluation and binding mode analysis. *Eur. J. Med. Chem.* **2019**, *166*, 304–317.

(44) Tahtouh, T.; Elkins, J. M.; Filippakopoulos, P.; Soundararajan, M.; Burgoyne, G.; Durieu, E.; Cochet, C.; Schmid, R. S.; Lo, D. C.; Delhomme, F.; Oberholzer, A. E.; Pearl, L. H.; Carreaux, F.; Bazureau, J.-P.; Knapp, S.; Meijer, L. Selectivity, cocrystal structures, and neuroprotective properties of leucettines, a family of protein kinase inhibitors derived from the marine sponge alkaloid leucettamine b. *J. Med. Chem.* **2012**, *55*, 9312–9330.

(45) Falke, H.; Chaikuad, A.; Becker, A.; Loaëc, N.; Lozach, O.; Abu Jhaisha, S.; Becker, W.; Jones, P. G.; Preu, L.; Baumann, K.; Knapp, S.; Meijer, L.; Kunick, C. 10-iodo-11h-indolo[3,2-c]quinoline-6-carboxylic acids are selective inhibitors of dyrk1a. *J. Med. Chem.* **2015**, *58*, 3131–3143.

(46) Czarna, A.; Wang, J.; Zelencova, D.; Liu, Y.; Deng, X.; Choi, H. G.; Zhang, T.; Zhou, W.; Chang, J. W.; Kildalsen, H.; Seternes, O. M.; Gray, N. S.; Engh, R. A.; Rothweiler, U. Novel scaffolds for dual

specificity tyrosine-phosphorylation-regulated kinase (dyrk1a) inhibitors. *J. Med. Chem.* **2018**, *61*, 7560–7572.

(47) Fruit, C.; Couly, F.; Bhansali, R.; Rammohan, M.; Lindberg, M. F.; Crispino, J. D.; Meijer, L.; Besson, T. Biological characterization of 8-cyclopropyl-2-(pyridin-3-yl)thiazolo[5,4-f]quinazolin-9(8h)-one, a promising inhibitor of dyrk1a. *Pharmaceuticals* **2019**, *12*, 185.

(48) Rothweiler, U.; Stensen, W.; Brandsdal, B. O.; Isaksson, J.; Leeson, F. A.; Engh, R. A.; Svendsen, J. S. M. Probing the atp-binding pocket of protein kinase dyrk1a with benzothiazole fragment molecules. *J. Med. Chem.* **2016**, *59*, 9814–9824.

(49) Otwinowski, Z.; Minor, W. Denzo and scalepack. In *International tables for crystallography volume f: Crystallography of biological macromolecules*; Rossmann, M. G., Arnold, E., Eds.; Springer Netherlands: Dordrecht, 2001; pp 226–235.

(50) Kabsch, W. Xds. *Acta Crystallogr. Sect. D Biol. Crystallogr.* **2010**, *66*, 125–132.

(51) Vagin, A.; Teplyakov, A. Molecular replacement withMOLREP. *Acta Crystallogr. Sect. D Biol. Crystallogr.* **2010**, *66*, 22–25.

(52) Murshudov, G. N.; Vagin, A. A.; Dodson, E. J. Refinement of macromolecular structures by the maximum-likelihood method. *Acta Crystallogr. Sect. D Biol. Crystallogr.* **1997**, *53*, 240–255.

(53) Winn, M. D.; Ballard, C. C.; Cowtan, K. D.; Dodson, E. J.; Emsley, P.; Evans, P. R.; Keegan, R. M.; Krissinel, E. B.; Leslie, A. G. W.; McCoy, A.; McNicholas, S. J.; Murshudov, G. N.; Pannu, N. S.; Potterton, E. A.; Powell, H. R.; Read, R. J.; Vagin, A.; Wilson, K. S. Overview of theCCP4 suite and current developments. *Acta Crystallogr. Sect. D Biol. Crystallogr.* **2011**, *67*, 235–242.

(54) Emsley, P.; Cowtan, K. Coot: model-building tools for molecular graphics. *Acta Crystallogr. Sect. D Biol. Crystallogr.* **2004**, *60*, 2126–2132.

(55) Schüttelkopf, A. W.; van Aalten, D. M. F.; Prodrig, D. M. F. PRODRG: a tool for high-throughput crystallography of protein-ligand complexes. *Acta Crystallogr. Sect. D Biol. Crystallogr.* **2004**, *60*, 1355–1363.